Molecular Therapy
Oncology
Original Article

CDKN2A copy number alteration in bladder cancer: Integrative analysis in patient-derived xenografts and cancer patients

Maria-Alexandra Papadimitriou,[1] Katerina-Marina Pilala,[1] Konstantina Panoutsopoulou,[1] Panagiotis Levis,[2] Georgios Kotronopoulos,[2] Zoi Kanaki,[3] Gedeon Loules,[4] Maria Zamanakou,[4] Dimitrios Linardoutsos,[5] Diamantis C. Sideris,[1] Konstantinos Stravodimos,[2] Apostolos Klinakis,[3] Andreas Scorilas,[1] and Margaritis Avgeris[1,6]

[1]Department of Biochemistry and Molecular Biology, Faculty of Biology, National and Kapodistrian University of Athens, Athens, Greece; [2]First Department of Urology, "Laiko" General Hospital, School of Medicine, National and Kapodistrian University of Athens, 115 27 Athens, Greece; [3]Biomedical Research Foundation Academy of Athens, Athens, Greece; [4]CeMIA SA, Larissa, Greece; [5]First Department of Propaedeutic Surgery, School of Medicine, National and Kapodistrian University of Athens, Athens, Greece; [6]Laboratory of Clinical Biochemistry – Molecular Diagnostics, Second Department of Pediatrics, School of Medicine, National and Kapodistrian University of Athens, "P. & A. Kyriakou" Children's Hospital, Athens, Greece

Bladder cancer (BlCa) is an extensively heterogeneous disease that leads to great variability in tumor evolution scenarios and lifelong patient surveillance, emphasizing the need for modern, minimally invasive precision medicine. Here, we explored the clinical significance of copy number alterations (CNAs) in BlCa. CNA profiling was performed in 15 patient-derived xenografts (PDXs) and validated in The Cancer Genome Atlas BlCa (TCGA-BLCA; *n* = 408) and Lindgren et al. (*n* = 143) cohorts. *CDKN2A* copy number loss was identified as the most frequent CNA in bladder tumors, associated with reduced CDKN2A expression, tumors of a papillary phenotype, and prolonged PDX survival. The study's screening cohort consisted of 243 BlCa patients, and *CDKN2A* copy number was assessed in genomic DNA and cell-free DNA (cfDNA) from 217 tumors and 189 pre-treatment serum samples, respectively. *CDKN2A* copy number loss was correlated with superior disease-free and progression-free survival of non-muscle-invasive BlCa (NMIBC) patients. Moreover, a higher *CDKN2A* index (*CDKN2A/LEP* ratio) in pre-treatment cfDNA was associated with advanced tumor stage and grade and short-term NMIBC progression to invasive disease, while multivariate models fitted for *CDKN2A* index in pre-treatment cfDNA offered superior risk stratification of T1/high-grade and EORTC high-risk patients, enhancing prediction of treatment outcome. *CDKN2A* copy number status could serve as a minimally invasive tool to improve risk stratification and support personalized prognosis in BlCa.

INTRODUCTION

Bladder cancer (BlCa) represents the third most prevalent malignancy, causing considerable morbidity and mortality rates among men in European countries.[1] The predominant histological type, urothelial bladder carcinoma (UBC; 90%), progresses through two distinct pathways that place significant challenges for clinical management. Non-muscle-invasive BlCa (NMIBC; 75%), although not considered life-threatening per se, exhibits high propensity rates for recurrence and progression to invasive stages, whereas muscle-invasive BlCa (MIBC; 25%) displays poor 5-year survival rates by frequently becoming metastatic and lethal.[2–4] Although several recent advancements in BlCa therapy have improved the response rates and patient survival, disease prognosis remains inadequate, and personalized treatment persists as a major medical need.[5,6] Notably, due to the high clinical heterogeneity, BlCa monitoring relies on procedure-based, lifelong follow-up strategies with medical imaging and invasive interventions, mainly cystoscopies, which have a severe impact on patient quality of life and impose the highest lifetime costs per patient to treat on healthcare systems.[7] Hence, novel molecular markers and minimally invasive liquid biopsy tools that can facilitate personalized prognosis and tailored therapeutics are of utmost clinical importance.[8]

Over the past decade, substantial progress has been achieved in understanding and elucidating the highly heterogeneous molecular landscape of bladder tumors.[9,10] Besides single-point mutations, gene-level copy number alterations (CNAs) are tightly intertwined with gene expression and tumor-related pathway regulation, being repeatedly associated with urothelial carcinoma development and progression[11–13] To date, recent technological advances have allowed

Received 9 October 2023; accepted 22 May 2024;
https://doi.org/10.1016/j.omton.2024.200818.

Correspondence: Andreas Scorilas, Department of Biochemistry and Molecular Biology, Faculty of Biology, National and Kapodistrian University of Athens, Panepistimiopolis, 15771 Athens, Greece.
E-mail: ascorilas@biol.uoa.gr
Correspondence: Margaritis Avgeris, Laboratory of Clinical Biochemistry - Molecular Diagnostics, Second Department of Pediatrics, "P. & A. Kyriakou" Children's Hospital, School of Medicine, National and Kapodistrian University of Athens, 24 Mesogeion Ave, 11527 Athens, Greece
E-mail: mavgeris@med.uoa.gr

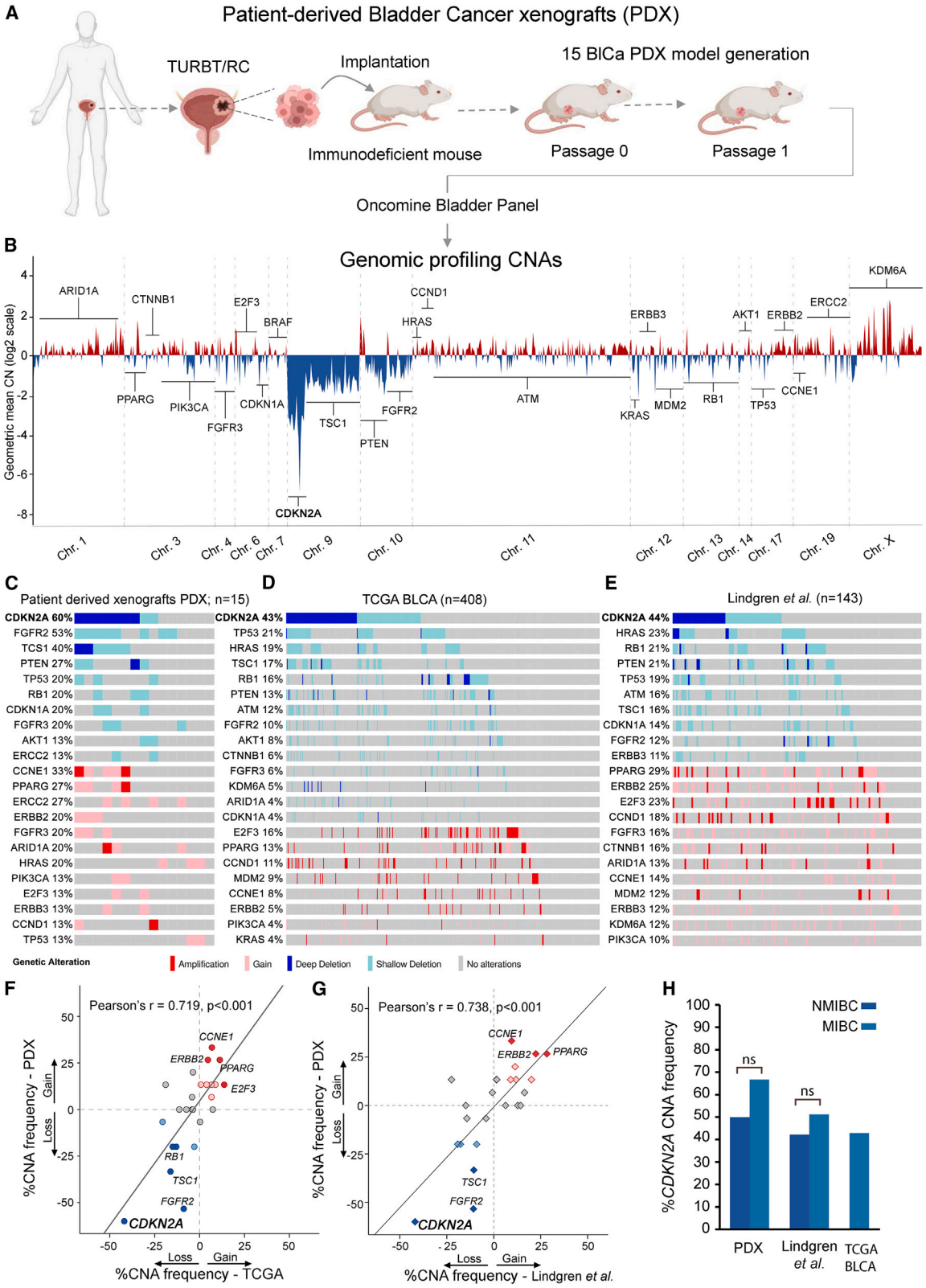

(legend on next page)

researchers to sensitively profile CNAs in both tumor genomic DNA (gDNA) and circulating cell-free DNA (cfDNA), providing a potent approach for the individual characterization of a patient's genomic spectrum and modern, minimally invasive disease prognosis and monitoring.[14–16] However, there is still limited understanding and exploitation in the clinical setting for BlCa patients.

In the present study, we explored CNAs landscape in urothelial bladder tumors, utilizing both patient-derived xenograft (PDX) mouse models and BlCa patients, highlighting, for the first time, the copy number loss of *CDKN2A* (cyclin-dependent kinase inhibitor 2A) as a potent, minimally invasive tool to improve patient risk stratification and support personalized disease prognosis. In this regard, CNA profiling of 15 PDXs and 2 external validation cohorts (The Cancer Genome Atlas [TCGA]-BLCA, n = 408;[17] Lindgren et al., n = 143[18]) revealed *CDKN2A* copy number loss as the most frequent alteration of bladder tumors, correlated with reduced *CDKN2A* expression, tumors of a papillary phenotype, and favorable PDX survival. To support expansion into clinical practice, CNAs of *CDKN2A* were analyzed in gDNA of bladder tumors and pre-treatment cfDNA in a screening cohort of 243 BlCa patients. Our findings highlighted that *CDKN2A* copy number loss, both in tumors and cfDNA, serves as a powerful independent predictor of NMIBC progression to invasive disease following treatment.

RESULTS

Profiling of CNAs in BlCa PDXs

Bladder tumor specimens were grafted in NOD.Cg-Prkdcscid Il2rgtm1Wjl/SzJ (NSG) mice to successfully generate 15 BlCa-PDX models (6 NMIBC, 9 MIBC). CNA profiling of PDX models was performed by DNA-sequencing (DNA-seq) (Figure 1A) and highlighted a wide chromosome 9 loss, with the most deep deletion spanning the *CDKN2A* gene locus on 9p21 (Figure 1B). Downstream analysis revealed that the most frequent focal homozygous deletion (HD) and loss of heterozygosity (LOH) events, were identified in the *CDKN2A* (60%), *FGFR2* (53%), *TSC1* (40%), *PTEN* (27%), *RB1* (20%), *TP53* (20%), and *CDKN1A* (20%) genes, while gains and focal amplifications were observed in the *CCNE1* (33%), *ERCC2* (27%), *PPARG* (27%), *ARID1A* (20%), *HRAS* (20%), *FGFR3* (20%), *ERBB2* (20%), *CCND1* (13%), and *E2F3* (13%) genes (Figure 1C). PDX analysis demonstrated the loss (HD/LOH) of the *CDKN2A* gene locus as the most frequent CNA, which was homozygous deleted in 7 (HD: 46.7%) and heterozygous deleted in 2 (LOH: 13.3%) PDX models (Figure S1).

To confirm our data, the TCGA-BLCA and Lindgren et al. cohorts were analyzed as validation cohorts. TCGA-BLCA analysis confirmed *CDKN2A* copy number loss (HD/LOH, 43%) as the most frequent CNA in bladder tumors, followed by *TP53* (21%), *HRAS* (19%), *TSC1* (17%), *RB1* (16%), *PTEN* (13%), *ATM* (12%), and *FGFR2* (10%) focal losses, while the most commonly amplified genes were *E2F3* (16%), *PPARG* (13%), *CCND1* (11%), and *MDM2* (9%) (Figure 1D). Similarly, in the Lindgren et al. cohort, *CDKN2A* copy number loss (44%) was the most common alteration, followed by focal losses of *HRAS* (23%), *RB1* (21%), *PTEN* (21%), and *TP53* (19%) and gains of *PPARG* (29%), *ERBB2* (25%), *E2F3* (23%), and *CCND1* (18%) (Figure 1E). The high concordance between PDX and validation datasets (PDX vs. TCGA-BLCA: r = 0.719, $p < 0.001$; PDX vs. Lindgren et al.: r = 0.738, $p < 0.001$; Figures 1F and 1G) confirmed that PDX models mirrored the CNA landscape of primary bladder tumors. Interestingly, *CDKN2A* displayed the highest HD rates (PDX: 46.7%, TCGA-BLCA: 22.6%, Lindgren et al., 21.3%), demonstrating the frequent complete loss of the *CDKN2A* gene locus in urothelial malignancy, while a similar distribution of *CDKN2A* deletions was observed between NMIBC and MIBC patients (Figures 1C–1E, 1H, and S1).

CDKN2A analysis in PDX models

CDKN2A copy number loss (HD/LOH) exhibited profound effects on *CDKN2A* expression in PDX models and the TCGA-BLCA and Lindgren et al. cohorts, as significantly lower CDKN2A mRNA and protein levels were detected in bladder tumors harboring *CDKN2A* HD/LOH compared to wild-type (WT) tumors (Figures 2A–2C). Focusing on the survival of PDX models, although marginally not significant (p = 0.062), *CDKN2A* loss was correlated with prolonged survival probability (Figure 2D). Survival analysis based on *CDKN2A* expression displayed similar results (p = 0.066), affirming that reduced *CDKN2A* expression and copy number loss were both correlated with superior PDX survival (Figure 2E). Moreover, the association of *CDKN2A* copy number status with the most recent molecular classification system of the TCGA-BLCA dataset (consensusMIBC 2020)[12] unveiled the significant prevalence of *CDKN2A* copy number loss and lower *CDKN2A* expression in luminal papillary (LumP) tumors, which are characterized by superior prognosis compared to other subtypes ($p < 0.001$; Figures 2F and 2G).

CDKN2A copy number loss in the bladder tumor molecular background and chemotherapy response

Our results demonstrated the association of *CDKN2A* copy number loss with tumors of papillary phenotype and superior disease prognosis, prompting us to get further insights into the role of *CDKN2A* copy number loss in the bladder tumor molecular landscape and treatment response. In this regard, we utilized Cancer Dependency Map (DepMap; https://depmap.org/portal/) to assess the correlation of *CDKN2A* copy number status with the sensitivity/resistance of 32 BlCa cell lines (Figure 3A) to the most commonly used systemic

Figure 1. CNA analysis of PDX mouse models

(A) Study design of PDX generation and CNA profiling. (B) CNA profiles of PDXs across the genome. Copy number losses are shown in blue and copy number gains in red. (C–E) Oncoplots of CNAs in PDX tumors (C) and the TCGA-BLCA (D) and Lindgren et al. (E) cohorts. (F and G) Pearson correlation dot plot of CNA frequency (%) between the PDX and TCGA-BLCA (F) and between the PDX and Lindgren et al. (G) cohorts. (H) Bar graph of *CDKN2A* CNA frequency (%) in the NMIBC and MIBC of PDX models and the Lindgren et al. and TCGA-BLCA cohorts. Oncoplots were generated by the cBioPortal Oncoprinter tool.

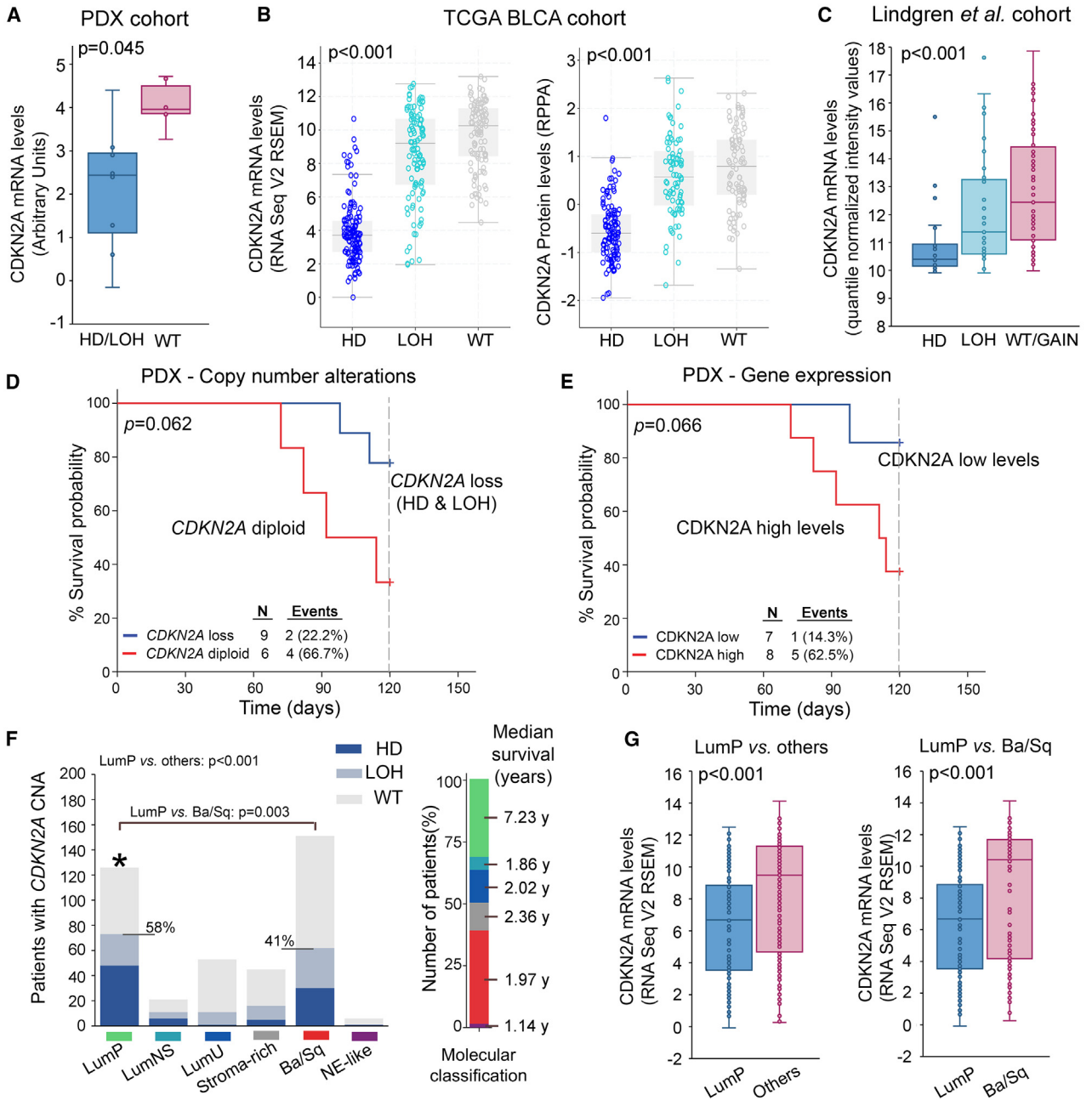

Figure 2. *CDKN2A* copy number status in bladder tumors

(A–C) Boxplots presenting the correlation of *CDKN2A* copy number loss (HD/LOH) with mRNA expression across PDX samples (A), mRNA and protein levels in the TCGA-BLCA cohort (B), and mRNA levels in the Lindgren et al. cohort (C). The *p* values were calculated by Mann-Whitney *U* (A) and Kruskal-Wallis (B and C) tests. (D and E) Kaplan-Meier survival curves of PDX mouse models according to *CDKN2A* copy number status (D) and *CDKN2A* mRNA levels (E). The *p* value was calculated by log rank test. (F) Bar graphs of *CDKN2A* copy number status distribution across the molecular subtypes (consensusMIBC 2020) of the TCGA-BLCA cohort. The *p* values were evaluated by Fisher's exact test. (G) Boxplots presenting the correlation of *CDKN2A* expression between LumP vs. other subtypes and LumP vs. Ba/Sq subtypes. The *p* values were calculated by Mann-Whitney *U* test.

chemotherapy drugs in BlCa treatment. BlCa cell lines harboring *CDKN2A* copy number loss were confirmed to express significantly reduced CDKN2A mRNA ($p < 0.001$; Figure 3B) and protein levels ($p < 0.001$; Figures 3B and 3C). Moreover, a significantly lower area under the dose-response curve (AUC; gemcitabine: $r_s = 0.675$, $p = 0.008$ [Figure 3D]; methotrexate: $r_s = 0.376$, $p = 0.124$ [Figure 3G];

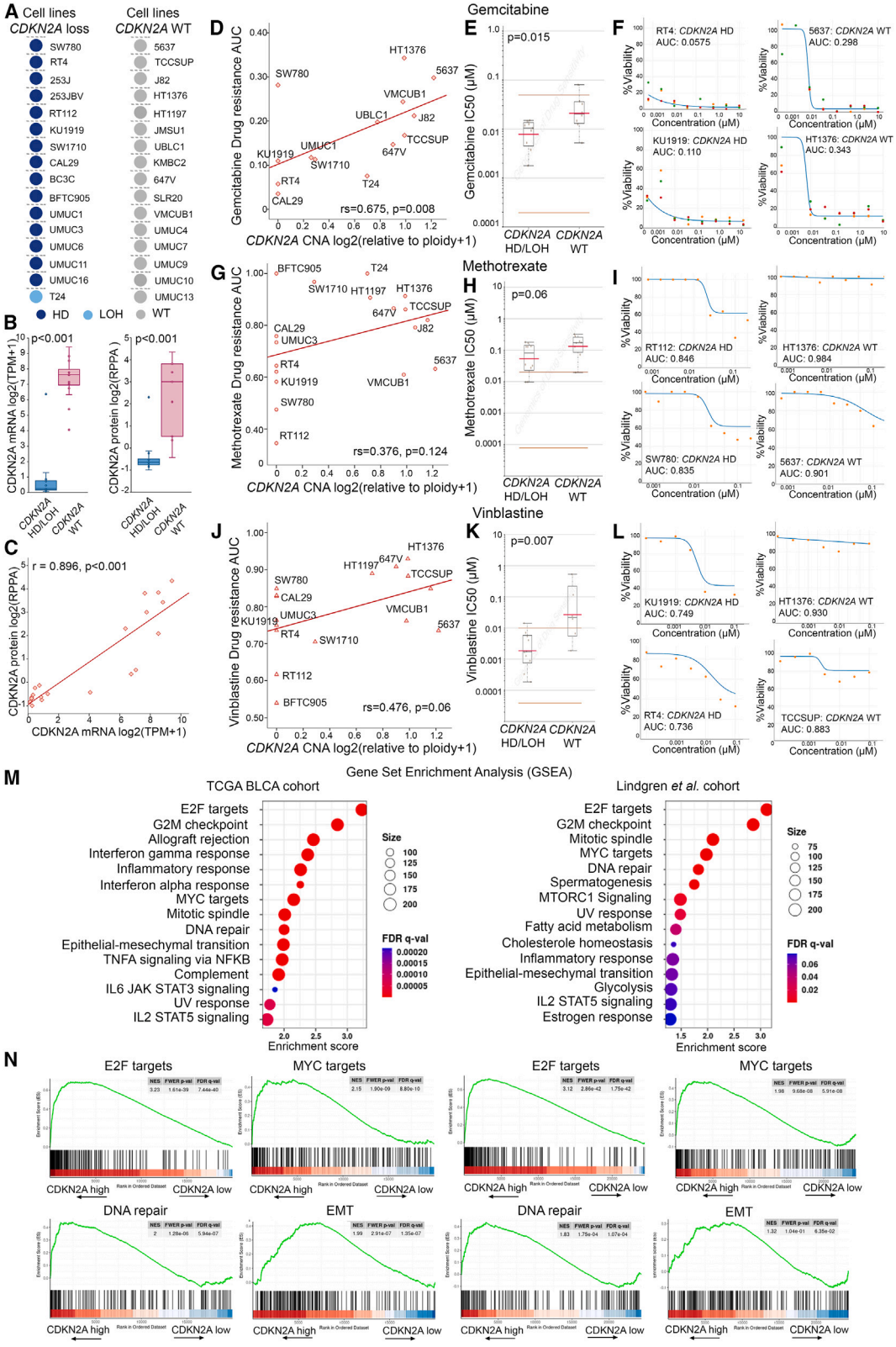

(legend on next page)

vinblastine: $r_s = 0.476$, $p = 0.060$ [Figure 3J]) and IC50 (half-maximal inhibitory concentration) values (gemcitabine: $p = 0.015$ [Figure 3E]; methotrexate: $p = 0.060$ [Figure 3H]; vinblastine: $p = 0.007$ [Figure 3K]) were documented for BlCa cells with *CDKN2A* copy number loss compared to WT ones, highlighting their increased sensitivity to gemcitabine (Figures 3D–3F), methotrexate (Figures 3G–3I), and vinblastine. Indicative dose-response curves of cell lines with *CDKN2A* copy number loss (e.g., RT4, RT112, KU1919, and SW780) compared to WT cells (e.g., 5637, HT1376, and TCCSUP) for gemcitabine, methotrexate, and vinblastine are displayed in Figures 3F, 3I, and 3L, respectively.

Moreover, gene set enrichment analysis (GSEA) was performed, utilizing the TCGA-BLCA and Lindgren et al. datasets. Intriguingly, apart from highlighting the role of CDKN2A in G2/M checkpoint state, our analysis revealed the significant CDKN2A-related enrichment of hallmark oncogenic gene sets, including E2F and MYC targets as well as DNA repair and epithelial-to-mesenchymal transition (EMT), underlying the potential involvement of *CDKN2A* in BlCa progression (Figures 3M and 3N).

CDKN2A copy number loss was associated with prolonged event-free survival of NMIBC patients

Motivated by our findings, we studied the clinical value of *CDKN2A* copy number status in a screening cohort of 243 BlCa patients, analyzing both patient tumors ($n = 217$) and pre-treatment serum samples ($n = 189$). Our qPCR-based quantification of *CDKN2A* copy number status displayed 100% concordance with both the DNA-seq data of the 15 PDX models and the known *CDKN2A* status (NCI-60/UBC-40 cell line panels) of 10 different cancer cell lines (Figures 4A and S2).[19,20] In our screening cohort, *CDKN2A* copy number loss was observed in 37.8% (HD: $n = 20$, LOH: $n = 62$) of the patient bladder tumors, while *CDKN2A* losses were equally distributed between NMIBC (39.2%) and MIBC (35.6%) patients (Figure 4C). Figure 4B presents the REporting recommendations for tumour MARKer prognostic studies (REMARK) diagram of our clinical study, while detailed clinicopathological features of the patients are summarized in Table 1.

Kaplan-Meier and Cox regression analyses were performed to evaluate the clinical significance of *CDKN2A* copy number loss for the post-treatment outcome of BlCa patients (Figure 5; Tables S1 and S2). Due to the diverse disease courses, survival analysis was performed separately in the NMIBC and MIBC patients, using tumor relapse and progression as well as metastasis/progression and mortality as clinical endpoints, respectively. NMIBC patients harboring *CDKN2A* copy number loss (HD/LOH) displayed superior disease-free survival (DFS) ($p = 0.015$; Figure 5A) and progression-free survival (PFS) ($p = 0.028$; Figure 5B) compared to *CDKN2A* diploid/gain patients, supporting the favorable prognostic value of *CDKN2A* loss observed in the PDX mouse models. In this regard, univariate Cox proportional regression analysis verified the significantly higher risk for short-term disease recurrence (hazard ratio [HR] = 2.168, $p = 0.010$; Figure 5C) and progression (HR = 2.834, $p = 0.018$; Figure 5E) of the *CDKN2A* diploid/gain NMIBC patients. Moreover, *CDKN2A* copy number status was highlighted as an independent predictor of NMIBC relapse (HR = 2.320, $p = 0.013$; Figure 5D) and progression to invasive disease stages (HR = 3.069, $p = 0.017$; Figure 5F) by multivariate Cox regression models adjusted for tumor stage, grade, patient gender, and age. Separate evaluation of HD vs. LOH *CDKN2A* status revealed that TaT1 patients harboring HD presented significantly extended PFS intervals ($p = 0.048$; Figure S3), and none of the *CDKN2A* HD patients displayed disease progression within their follow-up time compared to LOH and diploid/gain patients. Finally, the analysis did not reveal any significant predictive value of *CDKN2A* copy number status for MIBC (Figure S4; Table S2), highlighting its specific nature for NMIBC outcome.

Clinical utility of *CDKN2A* copy number status in pre-treatment cfDNA

The powerful prognostic significance of *CDKN2A* copy number status in bladder tumors prompted us to exploit its clinical value in patient pre-treatment cfDNA. The analysis highlighted the association of a higher *CDKN2A* index (*CDKN2A/LEP* ratio) in pre-treatment cfDNA with muscle-invasive (T2–T4) compared to superficial tumors (TaT1) ($p < 0.001$; Figure 6A) as well as with higher pathological tumor stages ($p < 0.001$; Figure 6B) and grade ($p \leq 0.001$; Figures 6C and 6D).

Moreover, Kaplan-Meier (Figures 6 and S5) and Cox regression (Figure 6; Tables S3 and S4) analyses were performed to evaluate the clinical significance of the *CDKN2A* index in pre-treatment cfDNA for disease course. In line with the results in tumor specimens, both Kaplan-Meier curves ($p = 0.012$; Figure 6E) and univariate Cox regression analysis (HR = 2.954; $p = 0.013$; Figure 6F) clearly illustrated the notably higher risk for short-term progression to invasive disease of TaT1 patients with a higher *CDKN2A* index. Finally,

Figure 3. *In silico* analysis of *CDKN2A* copy number loss in the bladder tumor molecular background and chemotherapy response

(A) *CDKN2A* copy number status of BlCa cell lines in the DepMap portal (https://depmap.org/portal/). (B) Boxplots presenting the correlation of *CDKN2A* copy number loss (HD/LOH) with mRNA and protein expression across BlCa cells. (C) Spearman correlation of CDKN2A mRNA and protein levels in BlCa cells. (D–L) Correlation of *CDKN2A* CNA with area under the dose-response curve (AUC) and IC50 values of BlCa cell lines for gemcitabine (D and E), methotrexate (G and H), and vinblastine (J and K). The *p* values were calculated by Mann-Whitney *U* test (B, E, H, and K) and Spearman analysis (C, D, G, and J). Shown are indicative dose-response curves of BlCa cells with *CDKN2A* copy number loss (e.g., RT4, RT112, KU1919, and SW780) compared to WT cells (e.g., 5637, HT1376, and TCCSUP) for gemcitabine (F), methotrexate (I), and vinblastine (L). (M) Dot plot of GSEA Hallmark analysis of the CDKN2A-related enriched gene sets in the TCGA-BLCA and Lindgren et al. cohorts. The size of the dots represents the number of genes, and the color of the dots represents the false discovery rate (FDR) q value. (N) Enrichment plots for the top four gene sets enriched in GSEA Hallmark analysis in the TCGA-BLCA and Lindgren et al. cohorts.

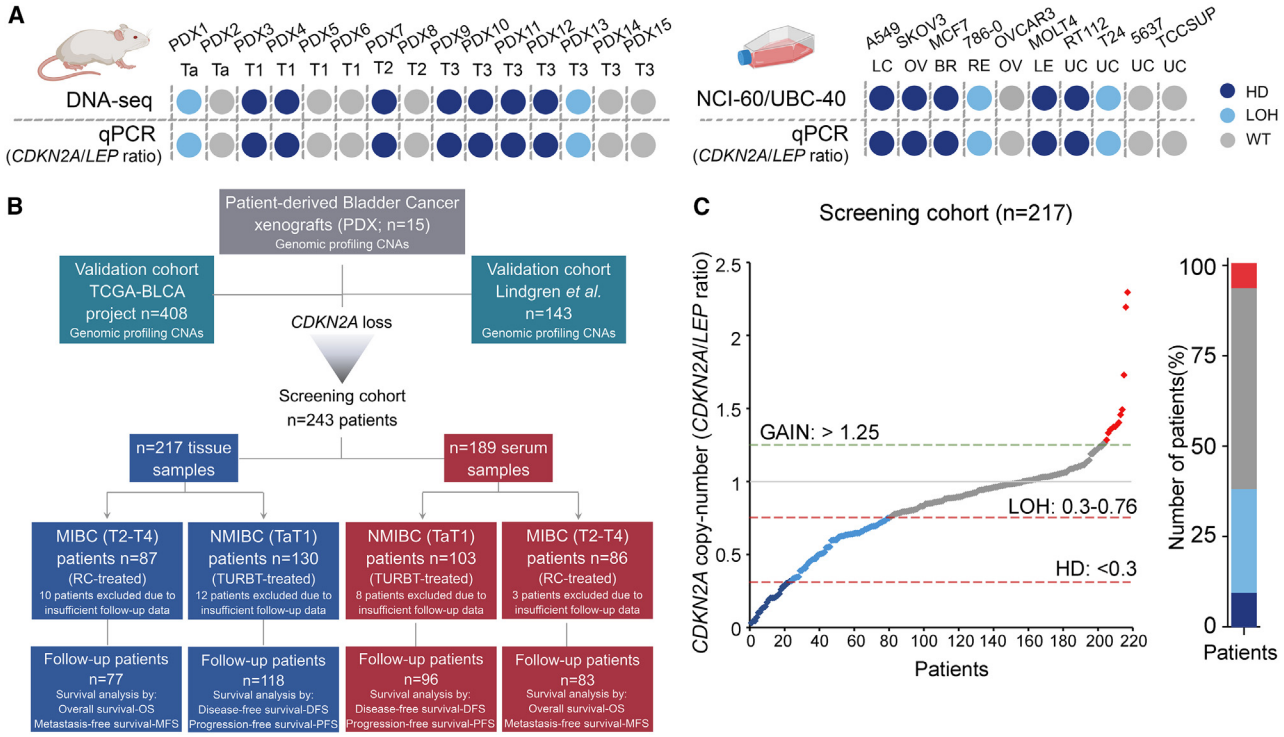

Figure 4. *CDKN2A* copy-number status screening in BlCa patients

(A) Comparison of *CDKN2A* copy number status between DNA-seq and qPCR in PDX models (left) and NCI-60/UBC-40 cell line panels and qPCR in 10 selected cell lines (right). (B) REMARK diagram of the study. (C) Distribution of *CDKN2A* copy number status in tumors of our BlCa screening cohort.

multivariate Cox models, adjusted for tumor stage, grade, patient gender, and age, clearly confirmed the worse prognosis of NMIBC patients with a higher cfDNA *CDKN2A* index independent of the clinically used disease markers (HR = 2.616, $p = 0.039$; Figure 6G). Similar to tumor *CDKN2A* status, the survival analysis did not highlight any statistically significant correlation with MIBC outcome (Table S4).

Analysis of *CDKN2A* copy number status in pre-treatment cfDNA improves the prognostic value of the established and clinical used disease markers

The independent clinical value of *CDKN2A* index in cfDNA for NMIBC outcome prompted us to evaluate its ability to strengthen the prognostic significance of the established disease markers. Multivariate models integrating cfDNA *CDKN2A* index with disease clinical markers clearly offered superior risk stratification and positive prediction of NMIBC progression to muscle-invasive disease (Figure 7). In this regard, the elevated *CDKN2A* index in pre-treatment cfDNA effectively distinguished T1HG patients at higher risk for progression ($p = 0.001$; Figure 7A). Similarly, a higher cfDNA *CDKN2A* index was associated with short-term progression among European Organisation of Research and Treatment of Cancer (EORTC) high-risk patients ($p = 0.020$; Figure 7B). Ultimately, decision curve analysis (DCA) analysis of cfDNA *CDKN2A* index-fitted multivariate prediction models, combining *CDKN2A* index with tumor stage, grade, and EORTC risk group clearly demonstrated the superior net benefit for the prediction of short-term progression of NMIBC patients compared to the control model of the established clinical markers alone (Figure 7C).

DISCUSSION

Despite the significant progress in BlCa therapy, the high rates of tumor recurrence/mortality and drug resistance remain major obstacles in efficient clinical management. An improved understanding of the genetic mechanisms underlying BlCa progression could be exploited to ameliorate non-invasive molecular diagnostics and tailored therapeutics.[21–23] Here, utilizing PDX mouse models and BlCa patient cohorts, we performed, for the first time, an integrative analysis of CNAs in bladder tumors and unveiled the clinical utility of both tumor and cfDNA copy number status of *CDKN2A* in improving personalized prognosis and prediction of BlCa patient treatment outcome.

DNA-seq of PDX models highlighted that *CDKN2A* displays the highest HD and LOH rates in UBC, which were further confirmed in the TCGA-BLCA and Lindgren et al. validation cohorts. Transcriptional analysis in both PDX models and validation cohorts revealed that *CDKN2A* copy number loss (HD/LOH) diminished *CDKN2A* expression and was associated with low-risk LumP tumors and prolonged PDX survival. Additionally, *CDKN2A* copy number loss was correlated with higher sensitivity of BlCa cells in gemcitabine,

Table 1. Detailed clinicopathological features of the screening cohort

	No. of patients (n = 243)	
Variable	BlCa gDNA cohort tissue (n = 217)	BlCa cfDNA cohort serum (n = 189)
Disease		
NMIBC (Ta, T1)	130 (59.9%)	103 (54.5%)
MIBC (T2–T4)	87 (40.1%)	86 (45.5%)
Tumor stage		
pTa	68 (31.3%)	53 (28.0%)
pT1	62 (28.6%)	50 (26.5%)
pT2	35 (16.1%)	33 (17.5%)
pT3/T4	51 (23.5%)	53 (28.0%)
Grade (WHO 2004)		
Low	80 (36.9%)	61 (32.3%)
High	137 (63.1%)	128 (67.7%)
Grade (WHO 1973)		
1	21 (9.7%)	20 (10.6%)
2	74 (34.1%)	52 (27.5%)
3	122 (56.2%)	117 (61.9%)
Gender		
Male	181 (83.4%)	154 (81.5%)
Female	36 (16.6%)	35 (18.5%)
NMIBC (TaT1)		
EORTC risk group		
Low risk	21 (16.2%)	18 (17.5%)
Intermediate risk	39 (30.0%)	29 (28.2%)
High risk	70 (53.8%)	56 (54.3%)
Disease monitoring		
Follow-up patients	118	96
Recurrence/progression	49 (41.5%)/26 (22.0%)	41 (42.7%)/23 (24.0%)
Mean DFS	46.57 months	45.71 months
Mean PFS	59.77 months	58.44 months
Excluded from follow-up	12	7
MIBC (T2–T4)		
Disease monitoring		
Follow-up patients	77	83
Progression/death	49 (63.6%)/43 (55.8%)	54 (65.1%)/48 (57.8%)
Mean DFS	50.82 months	48.62 months
Mean overall survival	58.43 months	55.53 months
Excluded from follow-up	10	3

methotrexate, and vinblastine, while GSEA of the TCGA-BLCA and Lindgren et al. cohorts highlighted the CDKN2A-related enrichment of hallmark oncogenic gene sets, including E2F and MYC targets as well as the G2M checkpoint, DNA repair, and EMT. Prompted by our results, we developed an in-house qPCR assay for the analysis of *CDKN2A* copy number status in our screening BlCa cohort, confirming the high prevalence of CDKN2A copy number loss in urothelial cancer. The survival analysis of our screening cohort demonstrated the superior prognosis and treatment outcome of TaT1 patients with *CDKN2A* deletions compared to *CDKN2A* diploid/gain patients, independent of the established disease markers and patient clinicopathological data, further validating the favorable prognostic utility of CDKN2A copy number loss observed in the PDX mouse models.

While cystoscopies are currently the gold-standard clinical tool for BlCa management, sampling restrictions may lead to tumor understaging and inadequate representation of disease heterogeneity, all while subjecting patients to invasive procedures.[24] In this regard, liquid biopsies hold great promise as new, minimally invasive tool, with significant implications in clinical practice. Given the potent clinical utility of *CDKN2A* copy number status in NMIBC prognosis, we further interrogated its value in pre-treatment patients' circulation. Notably, NMIBC patients with a high *CDKN2A* index in pre-treatment cfDNA were strongly associated with advanced tumor stage and grade, along with a significantly higher risk for short-term disease progression following transurethral tumor resection, independent of patients' clinicopathological data. In this regard, cfDNA *CDKN2A*-fitted multivariate models significantly ameliorated risk stratification and prognosis of NMIBC, resulting in the advanced positive prediction of disease progression within the clinically heterogeneous group of T1HG and EORTC-high risk patients. The superior risk stratification of NMIBC patients using cfDNA *CDKN2A*-fitted models could be applied in clinical practice and support personalized treatment/monitoring decision-making. In this regard, NMIBC patients at higher risk for progression to higher/invasive stages could be considered candidates for HR-like treatment/management by being subjected to prolonged intravesical bacillus Calmette-Guérin (BCG) administration (induction plus maintenance BCG for 3 years) or to immediate radical cystectomy (RC) in shared decision-making, also raising patients' awareness. Moreover, a risk-based follow-up strategy for NMIBC patients could also be utilized to reduce healthcare systems' economic burden and raise patients' quality of life.

CDKN2A encodes for the cycle-dependent kinases $p14^{ARF}$/$p16^{INK4A}$, while its activation has been closely associated with senescence.[25] In a clinical approach, the value of *CDKN2A* in BlCa prognostication has proven to be controversial. *CDKN2A* deletion and/or decreased $p16^{INK4A}$ expression has been documented to predict BlCa progression and lead to immune checkpoint therapy resistance.[26,27] However, new studies have highlighted a multifaceted role of *CDKN2A* in BlCa development. In this regard, and in line with our findings, *CDKN2A* copy number loss and/or reduced gene expression has been associated with luminal/papillary bladder tumors,[17,18,28] while $p14^{ARF}$/$p16^{INK4A}$ overexpression has been correlated with inferior survival expectancy of NMIBC patients and poor chemotherapy response of MIBC patients.[29–32]

Mechanistically, $p14^{ARF}$ and $p16^{INK4A}$ inhibit cell cycle progression and were initially described as potent tumor suppressors;[33] however,

Survival of NMIBC (TaT1) patients according to *CDKN2A* CNA

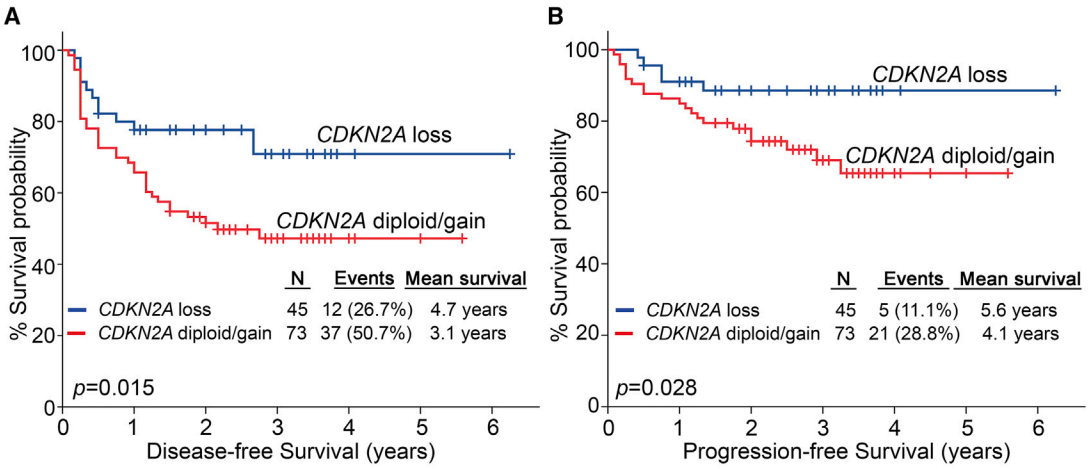

C Disease-free survival (DFS) — Univariate Cox regression analysis

Covariants: tested *vs.* control (HR=1)	HR	95% CI	*p*
CDKN2A CNA: Diploid/gain *vs.* Loss	2.168	(1.129 – 4.163)	0.010
Tumor Stage: T1 *vs.* Ta	1.371	(0.783 – 2.402)	0.267
Tumor Grade: High *vs.* Low	1.493	(0.848 – 2.632)	0.140
Gender: Female *vs.* Male	1.420	(0.636 – 3.170)	0.390
Age	0.997	(0.969 – 1.026)	0.830

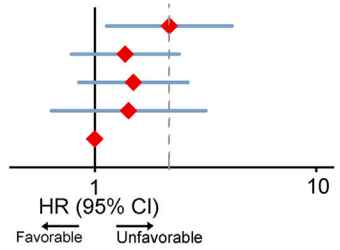

D Multivariate Cox regression analysis

Covariants: tested *vs.* control (HR=1)	HR	95% CI	*p*
CDKN2A CNA: Diploid/gain *vs.* Loss	2.320	(1.155 – 4.657)	0.013

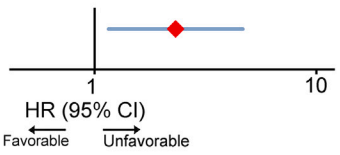

E Progression-free survival (PFS) — Univariate Cox regression analysis

Covariants: tested *vs.* control (HR=1)	HR	95% CI	*p*
CDKN2A CNA: Diploid/gain *vs.* Loss	2.834	(1.068 – 7.523)	0.018
Tumor Stage: T1 *vs.* Ta	1.685	(0.773 – 3.669)	0.168
Tumor Grade: High *vs.* Low	2.244	(1.037 – 4.853)	0.033
Gender: Female *vs.* Male	1.712	(0.587 – 4.996)	0.335
Age	1.013	(0.973 – 1.054)	0.493

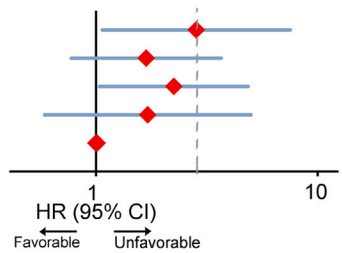

F Multivariate Cox regression analysis

Covariants: tested *vs.* control (HR=1)	HR	95% CI	*p*
CDKN2A CNA: Diploid/gain *vs.* Loss	3.069	(1.119 – 8.416)	0.017

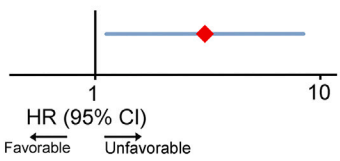

(legend on next page)

recent evidence has unveiled their pro-survival functions. In particular, $p14^{ARF}$-induced stabilization of FAK and SLUG, contributes to cervical and prostate cancer cell growth/proliferation, respectively, while human papillomavirus (HPV)-associated tumors induce $p16^{INK4A}$ expression to sustain their survival.[34–36] Moreover, senescent cancer cells are characterized by high levels of $p16^{INK4A}$,[37,38] and senolytic treatment strategies targeting $p16^{INK4A}$-high senescent cells efficiently increase the chemotherapy response and survival of glioblastoma- and breast cancer-bearing mice[39,40] Although the role of *CDKN2A* has not yet been clarified in bladder tumors, future studies will pave the way to unveil the causal link between its function and the strong clinical value in NMIBC prognosis and post-treatment outcome.

In conclusion, our study aimed to evaluate CNA emergence and clinical application in BlCa. Following the establishment and CNA profiling of PDX mouse models, *CDKN2A* copy number loss was highlighted as the most frequent CNA in bladder tumors and correlated with reduced *CDKN2A* expression, LumP tumors, and prolonged survival of the PDX models. The analysis of bladder tumors and pre-treatment cfDNA of the BlCa patient cohort clearly highlighted *CDKN2A* copy number status as a powerful independent indicator of NMIBC patient prognosis. Finally, we demonstrated that cfDNA *CDKN2A* index-fitted multivariate models offered superior risk stratification of NMIBC patients and improved prediction of post-treatment outcome compared to the clinically used disease markers, endorsing CNA analysis of *CDKN2A* in pre-treatment cfDNA for modern non-invasive precision medicine of BlCa patients.

MATERIALS AND METHODS

PDX mouse models

Primary bladder tumor samples (up to 5 mm, depending on tumor availability) were grafted subcutaneously in 6-week-old NSG mice (stock number 005557) obtained from The Jackson Laboratory (Bar Harbor, ME, USA). Mice were anesthetized with an intraperitoneal injection of a ketamine:xylazine solution (90 mg/kg ketamine and 10 mg/kg xylazine).[41] Tumors were allowed to reach a size up to 1 cm in diameter, and then mice were euthanized by cervical dislocation. During this period, tumor dimensions were measured weekly with calipers. Mice were closely monitored and sacrificed when tumors reached a size of 1 cm or displayed physical signs of discomfort, such as severe body weight loss or ulceration. The growth time from implantation varied from 1 to 7 months. Grafted tumors that failed to grow within 8 months (~30%) were considered "no take."[42] Harvested PDX tumors were snap frozen for future implantation and/or stored at −80°C for subsequent molecular analysis. Tumor segments for future implantation were placed in cryovials containing 1.5 mL of cryopreservation medium: 5% DMSO/95% fetal bovine serum (Sigma-Aldrich). Cryotubes were put in a freezing container containing isopropanol, placed in an −80°C freezer overnight, and transferred to a liquid nitrogen tank the next day. Mice were housed in individually ventilated cages under specific pathogen-free conditions at the Biomedical Research Foundation of the Academy of Athens (BRFAA) animal facility. All experiments were performed in compliance with national and international legislation and were approved by the BRFAA Committee of Ethics on Animal Experiments and the Attica Prefecture.

Screening cohort

The screening cohort of the study consisted of 243 patients diagnosed with primary BlCa at "Laiko" General Hospital (Athens, Greece). Fresh-frozen bladder tumors were obtained following transurethral resection of bladder tumor (TURBT) for NMIBC patients (TaT1) or RC for MIBC patients (T2–T4), while blood samples were collected prior to surgery. NMIBC patients received adjuvant treatment according to European Association of Urology (EAU) guidelines, while none of the patients received neoadjuvant therapy prior to surgery. Risk-group stratification of NMIBC patients was carried out according to EORTC guidelines. Based on EAU guidelines, post-treatment follow-up involved cystoscopy and urinary cytology for NMIBC patients or renal ultrasound and thoracoabdominal computed tomography CT/MRI every 3 and 6 months, respectively, for MIBC. If symptoms were observed, then supplemental CT/MRI, kidney ultrasound, and brain MRI/bone scans were performed. Tumor relapse (recurrence of an equal/lower pathologic stage) and progression (recurrence of a higher/invasive stage) of NMIBC was diagnosed by TURBT after positive cystoscopy results, while recurrence/metastasis of MIBC was affirmed by CT. During a median follow-up time of 35 months (95% confidence interval [CI]: 31.36–38.64), 221 patients were successfully followed up, whereas 22 patients were excluded due to insufficient monitoring data. Study approval was granted by the Ethics Committee of "Laiko" General Hospital. The study was conducted in compliance with the ethics standards of the 1975 Declaration of Helsinki, as revised in 2008. Before sample collection, all patients provided signed informed consent.

Validation cohorts

The TCGA (TCGA-BLCA project) and Lindgren et al. BlCa cohorts were utilized as validation cohorts of the study.[17,18] TCGA-BLCA consists of 412 patients diagnosed with UBC (n = 409, including 406 T2–T4 patients), papillary adenocarcinomas (n = 1), epithelial carcinomas (n = 1), and squamous cell carcinomas (n = 1). Affymetrix SNP6.0 arrays were used to assess CNAs, while mRNA expression profiles were generated by paired-end whole-transcriptome RNA sequencing (Illumina HiSeq platform). CNA and normalized RNA

Figure 5. *CDKN2A* copy number loss is associated with superior event-free survival of NMIBC patients

(A and B) Kaplan-Meier survival curves for disease-free survival (DFS; A) and progression-free survival (PFS; B) of the NMIBC cohort according to *CDKN2A* copy number status. The p values were calculated by log rank test. (C–F) Forest plots of the univariate and multivariate Cox regression analysis for DFS (C and D) and PFS (E and F) of NMIBC patients. Internal validation was performed by bootstrap Cox proportional regression analysis based on 1,000 bootstrap samples. HR, hazard ratio; 95% CI, 95% confidence interval of the estimated HR.

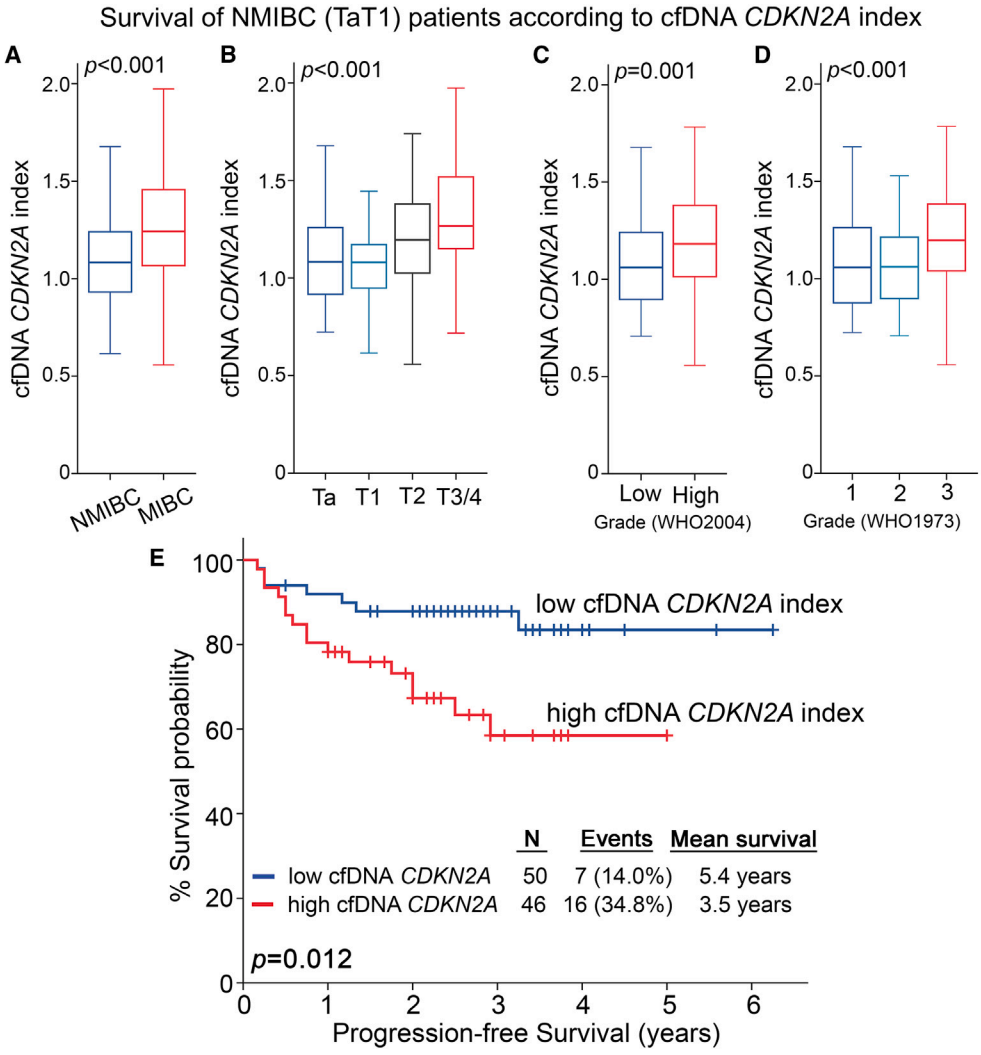

F

Progression-free survival (DFS)
Univariate Cox regression analysis

Covariants: tested *vs.* control (HR=1)	HR	95% CI	*p*
cfDNA *CDKN2A* index: High *vs.* Low	2.954	(1.210 – 7.210)	0.013
Tumor Stage: T1 *vs.* Ta	1.262	(0.557 – 2.861)	0.580
Tumor Grade: High *vs.* Low	1.908	(0.841 – 4.327)	0.117
Gender: Female *vs.* Male	0.998	(0.295 – 3.373)	0.997
Age	1.017	(0.976 – 1.059)	0.347

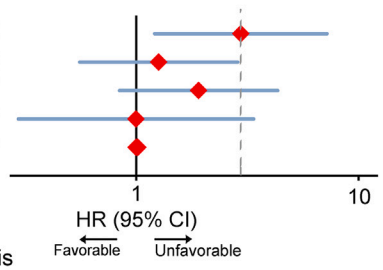

G

Multivariate Cox regression analysis

Covariants: tested *vs.* control (HR=1)	HR	95% CI	*p*
cfDNA *CDKN2A* index: High *vs.* Low	2.616	(1.040 – 6.582)	0.039

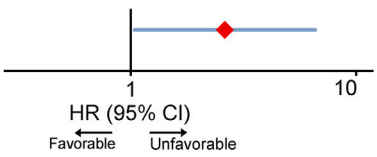

(legend on next page)

expression data along with the clinical data of the TCGA-BLCA project are available and can be explored through the Genomic Data Commons Data Portal (https://portal.gdc.cancer.gov/projects/TCGA-BLCA) and the Memorial Sloan Kettering Cancer Center cBioPortal (http://www.cbioportal.org). For the molecular classification of the TCGA-BLCA cohort, we utilized the unified consensus subtyping system (consensusMIBC 2020) proposed by Kamoun et al. that differentiates patients into 6 biologically relevant molecular classes; namely, LumP; luminal nonspecified; luminal unstable; stroma-rich, basal/squamous; and neuroendocrine-like.[12] The Lindgren et al. cohort includes 145 bladder tumor specimens [NMIBC = 102; MIBC = 42; Carcinoma *in situ* (Cis or Tis) = 1], submitted to genome tiling array [32K bacterial artificial chromosome (BAC) array], and gene expression array (Illumina HumanHT-12 v.3.0 expression beadchip) analysis for CNA and mRNA expression profiling, respectively. Publicly available clinical, can, and normalized RNA expression data were downloaded from the NCBI Gene Expression Omnibus (https://www.ncbi.nlm.nih.gov/geo/query/acc.cgi?acc=GSE32549).

Cell lines

A total of 10 human cell lines were used in the study: T24, TCCSUP, HTB-9, RT112 (BlCa), MCF-7 (breast cancer), OVCAR-3, SK-OV-3 (ovarian cancer), A549 (lung adenocarcinoma), MOLT-4 (acute T lymphoblastic leukemia), and 786-O (renal cell carcinoma). Each cell line was cultured according to the American Type Culture Collection instructions.

DNA extraction from tumors/cell lines and total RNA purification from PDX samples

gDNA from cell lines and patients/PDX tumor samples was isolated using TRI-Reagent (Molecular Research Center, Cincinnati, OH, USA) following homogenization of 5–10 $\times$ 10^6 cells or 40–100 mg of fresh-frozen tissue specimens, respectively. Prior to gDNA extraction, total RNA was also extracted from PDX samples using the phenol-chloroform method. According to the manufacturer's instructions, gDNA was dissolved and pH adjusted in 8 mM NaOH and 0.1 M HEPES buffer, total RNA was dissolved in RNA storage solution (Invitrogen, Carlsbad, CA, USA), and both analytes were stored at −80°C until analysis. The resulting DNA/RNA quality and concentration were assessed spectrophotometrically using a BioSpec Nano UV-visible spectrophotometer (Shimadzu, Kyoto, Japan).

cfDNA extraction from serum samples

5 mL of venous blood was sampled and allowed to clot at room temperature for 30 min before centrifugation at 1,200 $\times$ *g* for 20 min at 4°C. The serum supernatant was collected without disturbing the cellular layer and then stored at −80°C until analysis. Prior to cfDNA extraction, hemolyzed serum samples were excluded from the analysis by measuring spectrophotometrically free hemoglobin levels using the Harboe method and Allen correction. 500 µL of serum sample was used for total cfDNA extraction with the NucleoSpin cfDNA XS Kit (Macherey-Nagel, Düren, Germany) according to manufacturer's instructions. Total cfDNA quantification was performed fluorometrically on the Qubit 2.0 fluorometer (Life Technologies, Carlsbad, CA, USA) with the dsDNA HS Assay Kit (Life Technologies), while cfDNA fragment quantification and size distribution were assessed by capillary electrophoresis using the Agilent 2100 bioanalyzer (Agilent Technologies) with the Agilent High Sensitivity DNA Kit (Agilent Technologies, Santa Clara, CA, USA) according to the manufacturer's instructions.

DNA-seq

For each PDX sample, 10 ng of gDNA was amplified using the Oncomine Bladder Panel (Thermo Scientific) to construct DNA libraries using the Ion AmpliSeq Library Kit (Thermo Scientific). FuPa reagent was utilized to partially digest the primers, and the produced libraries were indexed with a unique adapter using the Ion Xpress Barcode Adapter Kit (Thermo Scientific). All barcoded libraries were purified using the Agencourt AMPure XP Beads (Beckman Coulter), quantified with a Qubit 4.0 fluorometer (Thermo Scientific), diluted to 50 pM, and pooled in equimolar proportions. Template preparation, enrichment, and chip loading were carried out on the Ion Chef system (Thermo Scientific). Sequencing was performed on S5XL, on a 530 chip, using the Ion 510 & Ion 520 & Ion 530 Kit-Chef Kit (Thermo Scientific). All procedures were performed according to the manufacturer's instructions.

Bioinformatics analysis

Base calling, demultiplexing, and alignment to the hg19 reference genome (GRCh37) of the sequencing raw data were performed on the Torrent Suite 5.10 software (Thermo Scientific) using default parameters. Variant calling was performed by the VariantCaller v.5.8.0.19 plug-in and coverage analysis by the coverageAnalysis v.5.8.0.8 plug-in in Torrent Suite 5.10. The data were further analyzed on Ion Reporter Software 5.18 for the detection and annotation of low-frequency somatic variants (SNPs, insertions or deletions, and CNAs) using the Oncomine Bladder – 530 – w4.2 – DNA – Single Sample workflow (v.4.2) and the Oncomine Extended (5.18) filter set. Quality control and coverage metrics of DNA-seq are included in Table S5.

In silico analysis

The GSEA software (Broad Institute, MA, USA) and MSigDB v.6.2 Hallmark gene set collection were used to identify the enrichment

Figure 6. High *CDKN2A* index in pre-treatment cfDNA is associated with worse prognosis

(A–D) Boxplots presenting the correlation of the *CDKN2A* index in pre-treatment cfDNA with patient tumor stage (A and B) and grade (C and D). The *p* values (two-sided) were calculated by Mann-Whitney *U* (A and C) and Kruskal-Wallis (B and D) tests. (E) Kaplan-Meier survival curve for the PFS of the NMIBC cohort according to *CDKN2A* index in pre-treatment cfDNA. The *p* value was calculated by log rank test. (F and G) Forest plots of the univariate and multivariate Cox regression analysis for the PFS of NMIBC patients. Internal validation was performed by bootstrap Cox proportional regression analysis based on 1,000 bootstrap samples.

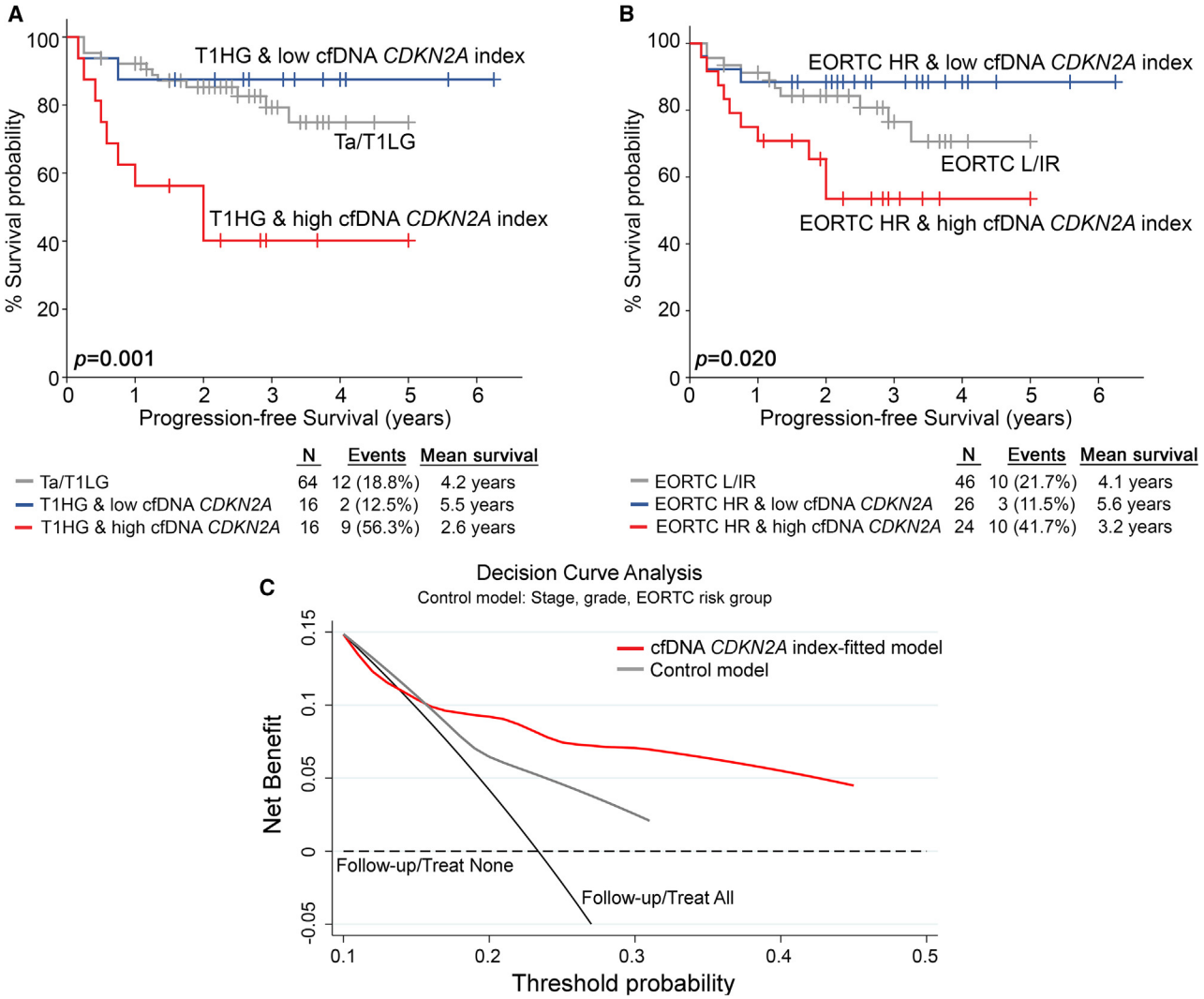

Figure 7. Evaluation of the *CDKN2A* index in pre-treatment cfDNA improves risk stratification and prediction of NMIBC progression to muscle-invasive disease

(A and B) Kaplan-Meier survival curves for the PFS of NMIBC patients according to *CDKN2A* index in pre-treatment cfDNA combined with tumor stage/grade (A) and EORTC risk group (B). The *p* values were calculated by log rank test. (C) DCA curves of "cfDNA *CDKN2A* index-fitted" and "control" multivariate prognostic models for the PFS of NMIBC patients. Net benefit is plotted against various ranges of threshold probabilities.

of CDKN2A-related gene sets in the TCGA-BLCA and Lindgren et al. cohorts. The GSEA software was assessed through Gene Enrichment Identifier (https://yoavshaul-lab.shinyapps.io/gsea-geni/).[43] Gene sets with absolute normalized enrichment score (NES) > 1.8 and false discovery rate (FDR) q < 0.05 were considered significant and reported.

CNA and mRNA expression profiling as well as response data to gemcitabine, methotrexate, and vinblastine of BlCa cell lines were obtained through the DepMap portal (https://depmap.org/portal) of the Broad Institute. The IC50 values represent the drug concentration that reduced cell viability by 50%, while the area under the AUC is calculated by plotting percent viability vs. drug concentration.

First-strand cDNA synthesis and *CDKN2A* expression quantification

Reverse transcription was performed in a 20-μL reaction by 50 U MMLV reverse transcriptase (Invitrogen), 40 U recombinant ribonuclease inhibitor (Invitrogen), and 5 μM oligo-deoxythymidine primer, using as template 1 μg of total RNA. Reverse transcription was performed at 37°C for 60 min, whereas enzyme was inactivated at 70°C for 15 min.

CDKN2A expression levels were quantified by SYBR-Green fluorescence-based quantitative PCR (qPCR). Based on published sequences, specific CDKN2A (GenBank: NM_058195.4, NM_000077.5;

F: 5′-GAAGGTCCCTCAGACATCCCC-3′, R: 5′-CCCTGTAGGAC CTTCGGTGAC-3′) and HPRT1 (GenBank: NM_000194.3; F: 5′-TG GAAAGGGTGTTTATTCCTCAT-3′, R: 5′- ATGTAATCCAGCAG GTCAGCAA-3′) primers were designed to produce specific 120-bp CDKN2A and 151-bp HPRT1 amplicons. The qPCR assays performed in the QuantStudio 5 Real-Time PCR System (Applied Biosystems) in 10-μL reactions consisted of Kapa SYBR Fast Universal 2× qPCR MasterMix (Kapa Biosystems, Woburn, MA, USA), 100 nM of each specific qPCR primer, and 10 ng of cDNA template. Polymerase activation was performed at 95°C for 3 min, followed by 40 cycles of a denaturation step at 95°C for 15 s and a primer annealing and extension step at 60°C for 1 min. Following amplification, melting curve analysis and agarose gel electrophoresis of the products were used for the discrimination of specific amplicons. *CDKN2A* expression was quantified by the $2^{-\Delta\Delta CT}$ relative quantification method, using *HPRT1* as an internal control for normalization purposes.

CDKN2A CNA analysis

CNAs of *CDKN2A* in gDNA and cfDNA samples were analyzed by a SYBR Green-based qPCR assay using *LEP* as the diploid reference gene. According to published sequences and *in silico* analysis, specific primers for the *CDKN2A* (NCBI: 1029; NC_000009.12; F: 5′-AT GCCTGCTTCTACAAACCCAC-3′, R: 5′-GGAGCCCATACGCA ACGAGAT-3′) and *LEP* (NCBI: 3952; NC_000007.14; F: 5′-CTC CACCCCATCCTGACCTTA-3′, R: 5′-AGGTTCTCCAGGTCGTT GGAT-3′) genes were designed for the amplification of specific 119-bp *CDKN2A* and 116-bp *LEP* amplicons. The qPCR assays were performed in 10-μL reactions that included Kapa SYBR Fast Universal 2× qPCR Master Mix (Kapa Biosystems), 200 nM of each PCR primer and 1 μL of gDNA or 300 nM of each PCR primer and 2 μL of cfDNA template in the 7500 Real-Time PCR System (Applied Biosystems). Polymerase activation was carried out at 95°C for 10 min, followed by 40 cycles of a denaturation step at 95°C for 30 s and a primer annealing and extension step at 60°C for 1 min. Thereafter, melting curve analysis and agarose gel electrophoresis were conducted to assess PCR amplicon specificity.

CDKN2A CNAs were calculated according to the $2^{-\Delta\Delta CT}$ relative quantification method, using *LEP* as the diploid reference gene.[44] Standard curves for the identification of the assays' limit of quantification and the determination of optimal cutoff values for *CDKN2A* homozygous/hemizygous deletions were constructed using diploid human gDNA as well as SK-OV-3 and RT112 cell line gDNA with known HD of *CDKN2A* (NCI-60/UBC-40 cell line panels[19,20,45]). All standard curve assays were performed in triplicate.

Statistical analysis

Statistical analysis was performed by SPSS Statistics 20 software (IBM, Armonk, NY, USA). Sapiro-Wilk and Kolmogorov-Smirnov tests were applied to test data's normal distribution. The non-parametric Mann-Whitney *U* and Kruskal-Wallis tests were used to assess the correlation of *CDKN2A* copy number status and expression with categorical clinicopathological features, while the association between TCGA consensus classes and *CDKN2A* CNAs was calculated by Fisher's exact tests. The similarity of CNA profiles between the PDX, TCGA-BLCA, and Lindgren et al. cohorts was evaluated by calculating the Pearson correlation of gene-level CNAs of the samples.

Kaplan-Meier survival curves using log rank test and Cox proportional regression analysis were implemented for patient survival analysis. The X-tile algorithm was applied for the optimal selection of the cutoff values of the cfDNA *CDKN2A* index (*CDKN2A/LEP* ratio). Internal validation was performed by bootstrap Cox proportional regression analysis based on 1,000 bootstrap samples. Finally, DCA was performed according to Vickers et al. by STATA 13 software (StataCorp, College Station, TX, USA) in order to evaluate the clinical benefit of the cfDNA *CDKN2A* index in patient treatment outcome.[46,47]

DATA AND CODE AVAILABILITY

Data supporting the findings of this study are available within the paper and its supplemental information. CNA and normalized RNA expression data along with the clinical data of the TCGA-BLCA project were acquired from the Genomic Data Commons Data Portal (https://portal.gdc.cancer.gov/projects/TCGA-BLCA) and the Memorial Sloan Kettering Cancer Center cBioPortal (http://www.cbioportal.org). Publicly available clinical, CNA, and normalized RNA expression data of the Lindgren et al. cohort were downloaded from the NCBI Gene Expression Omnibus (https://www.ncbi.nlm.nih.gov/geo/query/acc.cgi?acc=GSE32549). CNA data for the NCI-60 cell lines used in the study can be retrieved from CellMiner (https://discover.nci.nih.gov/cellminer/), while CNA data for UBC-40 cell lines are available in the Earl et al. study.[19] CNA, mRNA expression profiling, and drug response data of BlCa cell lines were obtained through the DepMap portal (https://depmap.org/portal) of the Broad Institute. All data are available from the corresponding authors upon reasonable request.

SUPPLEMENTAL INFORMATION

Supplemental information can be found online at https://doi.org/10.1016/j.omton.2024.200818.

ACKNOWLEDGMENTS

This research was co-financed by the European Regional Development Fund of the European Union and Greek national funds through the Operational Program Competitiveness, Entrepreneurship and Innovation under the call RESEARCH-CREATE-INNOVATE (project code: T2EDK-02196) to the National and Kapodistrian University of Athens (KE17358). The research work was supported by the Hellenic Foundation for Research and Innovation (HFRI) under the Third Call for HFRI PhD Fellowships (fellowship number 6123 to M.-A.P.).

AUTHOR CONTRIBUTIONS

M.-A.P., conceptualization and design, methodology, investigation, formal analysis, validation, visualization, data curation, and writing –

original draft; K.-M.P. and K.P., investigation; P.L., G.K., Z.K., G.L., M.Z., and D.L., investigation and resources; D.C.S. and K.S., resources and writing—review and editing; A.K., investigation, resources, and writing – review and editing; A.S., resources, writing – review and editing, project administration, and funding acquisition; M.A., conceptualization and design, methodology, investigation, formal analysis, validation, visualization, data curation, writing – review and editing, project administration, and supervision. All authors have read and agreed to the published version of the manuscript.

DECLARATION OF INTERESTS

The authors declare no competing interests.

REFERENCES

1. Sung, H., Ferlay, J., Siegel, R.L., Laversanne, M., Soerjomataram, I., Jemal, A., and Bray, F. (2021). Global Cancer Statistics 2020: GLOBOCAN Estimates of Incidence and Mortality Worldwide for 36 Cancers in 185 Countries. CA A Cancer J. Clin. *71*, 209–249.
2. Cambier, S., Sylvester, R.J., Collette, L., Gontero, P., Brausi, M.A., van Andel, G., Kirkels, W.J., Silva, F.C.D., Oosterlinck, W., Prescott, S., et al. (2016). EORTC Nomograms and Risk Groups for Predicting Recurrence, Progression, and Disease-specific and Overall Survival in Non-Muscle-invasive Stage Ta-T1 Urothelial Bladder Cancer Patients Treated with 1-3 Years of Maintenance Bacillus Calmette-Guérin. Eur. Urol. *69*, 60–69.
3. Messing, E.M., Tangen, C.M., Lerner, S.P., Sahasrabudhe, D.M., Koppie, T.M., Wood, D.P., Jr., Mack, P.C., Svatek, R.S., Evans, C.P., Hafez, K.S., et al. (2018). Effect of Intravesical Instillation of Gemcitabine vs Saline Immediately Following Resection of Suspected Low-Grade Non-Muscle-Invasive Bladder Cancer on Tumor Recurrence: SWOG S0337 Randomized Clinical Trial. JAMA *319*, 1880–1888.
4. Witjes, J.A., Bruins, H.M., Cathomas, R., Compérat, E.M., Cowan, N.C., Gakis, G., Hernández, V., Linares Espinós, E., Lorch, A., Neuzillet, Y., et al. (2021). European Association of Urology Guidelines on Muscle-invasive and Metastatic Bladder Cancer: Summary of the 2020 Guidelines. Eur. Urol. *79*, 82–104.
5. Tran, L., Xiao, J.F., Agarwal, N., Duex, J.E., and Theodorescu, D. (2021). Advances in bladder cancer biology and therapy. Nat. Rev. Cancer *21*, 104–121.
6. Williams, S.B., Howard, L.E., Foster, M.L., Klaassen, Z., Sieluk, J., De Hoedt, A.M., and Freedland, S.J. (2021). Estimated Costs and Long-term Outcomes of Patients With High-Risk Non-Muscle-Invasive Bladder Cancer Treated With Bacillus Calmette-Guérin in the Veterans Affairs Health System. JAMA Netw. Open *4*, e213800.
7. Clinton, T.N., Chen, Z., Wise, H., Lenis, A.T., Chavan, S., Donoghue, M.T.A., Almassi, N., Chu, C.E., Dason, S., Rao, P., et al. (2022). Genomic heterogeneity as a barrier to precision oncology in urothelial cancer. Cell Rep. *41*, 111859.
8. van Hoogstraten, L.M.C., Vrieling, A., van der Heijden, A.G., Kogevinas, M., Richters, A., and Kiemeney, L.A. (2023). Global trends in the epidemiology of bladder cancer: challenges for public health and clinical practice. Nat. Rev. Clin. Oncol. *20*, 287–304.
9. Guo, G., Sun, X., Chen, C., Wu, S., Huang, P., Li, Z., Dean, M., Huang, Y., Jia, W., Zhou, Q., et al. (2013). Whole-genome and whole-exome sequencing of bladder cancer identifies frequent alterations in genes involved in sister chromatid cohesion and segregation. Nat. Genet. *45*, 1459–1463.
10. Hurst, C.D., Platt, F.M., Taylor, C.F., and Knowles, M.A. (2012). Novel tumor subgroups of urothelial carcinoma of the bladder defined by integrated genomic analysis. Clin. Cancer Res. *18*, 5865–5877.
11. Sjodahl, G., Eriksson, P., Patschan, O., Marzouka, N.A., Jakobsson, L., Bernardo, C., Lovgren, K., Chebil, G., Zwarthoff, E., Liedberg, F., and Hoglund, M. (2020). Molecular changes during progression from nonmuscle invasive to advanced urothelial carcinoma. Int. J. Cancer *146*, 2636–2647.
12. Kamoun, A., de Reyniès, A., Allory, Y., Sjödahl, G., Robertson, A.G., Seiler, R., Hoadley, K.A., Groeneveld, C.S., Al-Ahmadie, H., Choi, W., et al. (2020). A Consensus Molecular Classification of Muscle-invasive Bladder Cancer. Eur. Urol. *77*, 420–433.
13. Taber, A., Christensen, E., Lamy, P., Nordentoft, I., Prip, F., Lindskrog, S.V., Birkenkamp-Demtröder, K., Okholm, T.L.H., Knudsen, M., Pedersen, J.S., et al. (2020). Molecular correlates of cisplatin-based chemotherapy response in muscle invasive bladder cancer by integrated multi-omics analysis. Nat. Commun. *11*, 4858.
14. Vandekerkhove, G., Lavoie, J.M., Annala, M., Murtha, A.J., Sundahl, N., Walz, S., Sano, T., Taavitsainen, S., Ritch, E., Fazli, L., et al. (2021). Plasma ctDNA is a tumor tissue surrogate and enables clinical-genomic stratification of metastatic bladder cancer. Nat. Commun. *12*, 184.
15. Soave, A., Chun, F.K.H., Hillebrand, T., Rink, M., Weisbach, L., Steinbach, B., Fisch, M., Pantel, K., and Schwarzenbach, H. (2017). Copy number variations of circulating, cell-free DNA in urothelial carcinoma of the bladder patients treated with radical cystectomy: a prospective study. Oncotarget *8*, 56398–56407.
16. Rose Brannon, A., Jayakumaran, G., Diosdado, M., Patel, J., Razumova, A., Hu, Y., Meng, F., Haque, M., Sadowska, J., Murphy, B.J., et al. (2021). Enhanced specificity of clinical high-sensitivity tumor mutation profiling in cell-free DNA via paired normal sequencing using MSK-ACCESS. Nat. Commun. *12*, 3770.
17. Robertson, A.G., Kim, J., Al-Ahmadie, H., Bellmunt, J., Guo, G., Cherniack, A.D., Hinoue, T., Laird, P.W., Hoadley, K.A., Akbani, R., et al. (2017). Comprehensive Molecular Characterization of Muscle-Invasive Bladder Cancer. Cell *171*, 540–556.e25.
18. Lindgren, D., Sjödahl, G., Lauss, M., Staaf, J., Chebil, G., Lövgren, K., Gudjonsson, S., Liedberg, F., Patschan, O., Månsson, W., et al. (2012). Integrated genomic and gene expression profiling identifies two major genomic circuits in urothelial carcinoma. PLoS One *7*, e38863.
19. Earl, J., Rico, D., Carrillo-de-Santa-Pau, E., Rodríguez-Santiago, B., Méndez-Pertuz, M., Auer, H., Gómez, G., Grossman, H.B., Pisano, D.G., Schulz, W.A., et al. (2015). The UBC-40 Urothelial Bladder Cancer cell line index: a genomic resource for functional studies. BMC Genom. *16*, 403.
20. Varma, S., Pommier, Y., Sunshine, M., Weinstein, J.N., and Reinhold, W.C. (2014). High resolution copy number variation data in the NCI-60 cancer cell lines from whole genome microarrays accessible through CellMiner. PLoS One *9*, e92047.
21. Sun, H., Cao, S., Mashl, R.J., Mo, C.K., Zaccaria, S., Wendl, M.C., Davies, S.R., Bailey, M.H., Primeau, T.M., Hoog, J., et al. (2021). Comprehensive characterization of 536 patient-derived xenograft models prioritizes candidates for targeted treatment. Nat. Commun. *12*, 5086.
22. Park, S., Rong, L., Owczarek, T.B., Bernardo, M.D., Shoulson, R.L., Chua, C.W., Kim, J.Y., Lankarani, A., Chakrapani, P., Syed, T., et al. (2021). Novel Mouse Models of Bladder Cancer Identify a Prognostic Signature Associated with Risk of Disease Progression. Cancer Res. *81*, 5161–5175.
23. Pilala, K.M., Papadimitriou, M.A., Panoutsopoulou, K., Barbarigos, P., Levis, P., Kotronopoulos, G., Stravodimos, K., Scorilas, A., and Avgeris, M. (2022). Epigenetic regulation of MIR145 core promoter controls miR-143/145 cluster in bladder cancer progression and treatment outcome. Mol. Ther. Nucleic Acids *30*, 311–322.
24. Caglic, I., Panebianco, V., Vargas, H.A., Bura, V., Woo, S., Pecoraro, M., Cipollari, S., Sala, E., and Barrett, T. (2020). MRI of Bladder Cancer: Local and Nodal Staging. J. Magn. Reson. Imag. *52*, 649–667.
25. Cancer Genome Atlas Research Network (2012). Comprehensive genomic characterization of squamous cell lung cancers. Nature *489*, 519–525.
26. Yurakh, A.O., Ramos, D., Calabuig-Fariñas, S., López-Guerrero, J.A., Rubio, J., Solsona, E., Romanenko, A.M., Vozianov, A.F., Pellin, A., and Llombart-Bosch, A. (2006). Molecular and immunohistochemical analysis of the prognostic value of cell-cycle regulators in urothelial neoplasms of the bladder. Eur. Urol. *50*, 506–515. discussion 515.
27. Han, G., Yang, G., Hao, D., Lu, Y., Thein, K., Simpson, B.S., Chen, J., Sun, R., Alhalabi, O., Wang, R., et al. (2021). 9p21 loss confers a cold tumor immune microenvironment and primary resistance to immune checkpoint therapy. Nat. Commun. *12*, 5606.
28. Iyer, G., Al-Ahmadie, H., Schultz, N., Hanrahan, A.J., Ostrovnaya, I., Balar, A.V., Kim, P.H., Lin, O., Weinhold, N., Sander, C., et al. (2013). Prevalence and co-occurrence of actionable genomic alterations in high-grade bladder cancer. J. Clin. Oncol. *31*, 3133–3140.
29. Raspollini, M.R., Luque, R.J., Menendez, C.L., Bollito, E., Brunelli, M., Martignoni, G., Montironi, R., Cheng, L., Blanca, A., Baroni, G., et al. (2016). T1 high-grade bladder

carcinoma outcome: the role of p16, topoisomerase-IIα, survivin, and E-cadherin. Hum. Pathol. *57*, 78–84.

30. Breyer, J., Wirtz, R.M., Erben, P., Worst, T.S., Stoehr, R., Eckstein, M., Bertz, S., Sikic, D., Denzinger, S., Burger, M., et al. (2018). High CDKN2A/p16 and Low FGFR3 Expression Predict Progressive Potential of Stage pT1 Urothelial Bladder Carcinoma. Clin. Genitourin. Cancer *16*, 248–256.e2.
31. Owczarek, T.B., Kobayashi, T., Ramirez, R., Rong, L., Puzio-Kuter, A.M., Iyer, G., Teo, M.Y., Sánchez-Vega, F., Wang, J., Schultz, N., et al. (2017). ARF Confers a Context-Dependent Response to Chemotherapy in Muscle-Invasive Bladder Cancer. Cancer Res. *77*, 1035–1046.
32. Worst, T.S., Weis, C.A., Stöhr, R., Bertz, S., Eckstein, M., Otto, W., Breyer, J., Hartmann, A., Bolenz, C., Wirtz, R.M., and Erben, P. (2018). CDKN2A as transcriptomic marker for muscle-invasive bladder cancer risk stratification and therapy decision-making. Sci. Rep. *8*, 14383.
33. Zhao, R., Choi, B.Y., Lee, M.H., Bode, A.M., and Dong, Z. (2016). Implications of Genetic and Epigenetic Alterations of CDKN2A (p16(INK4a)) in Cancer. EBioMedicine *8*, 30–39.
34. McLaughlin-Drubin, M.E., Park, D., and Munger, K. (2013). Tumor suppressor p16INK4A is necessary for survival of cervical carcinoma cell lines. Proc. Natl. Acad. Sci. USA *110*, 16175–16180.
35. Vivo, M., Fontana, R., Ranieri, M., Capasso, G., Angrisano, T., Pollice, A., Calabrò, V., and La Mantia, G. (2017). p14ARF interacts with the focal adhesion kinase and protects cells from anoikis. Oncogene *36*, 4913–4928.
36. Xie, Y., Liu, S., Lu, W., Yang, Q., Williams, K.D., Binhazim, A.A., Carver, B.S., Matusik, R.J., and Chen, Z. (2014). Slug regulates E-cadherin repression via p19Arf in prostate tumorigenesis. Mol. Oncol. *8*, 1355–1364.
37. Cohn, R.L., Gasek, N.S., Kuchel, G.A., and Xu, M. (2023). The heterogeneity of cellular senescence: insights at the single-cell level. Trends Cell Biol. *33*, 9–17.
38. Soureas, K., Papadimitriou, M.A., Panoutsopoulou, K., Pilala, K.M., Scorilas, A., and Avgeris, M. (2023). Cancer quiescence: non-coding RNAs in the spotlight. Trends Mol. Med. *29*, 843–858.
39. Demaria, M., O'Leary, M.N., Chang, J., Shao, L., Liu, S., Alimirah, F., Koenig, K., Le, C., Mitin, N., Deal, A.M., et al. (2017). Cellular Senescence Promotes Adverse Effects of Chemotherapy and Cancer Relapse. Cancer Discov. *7*, 165–176.
40. Salam, R., Saliou, A., Bielle, F., Bertrand, M., Antoniewski, C., Carpentier, C., Alentorn, A., Capelle, L., Sanson, M., Huillard, E., et al. (2023). Cellular senescence in malignant cells promotes tumor progression in mouse and patient Glioblastoma. Nat. Commun. *14*, 441.
41. Kanaki, Z., Voutsina, A., Markou, A., Pateras, I.S., Potaris, K., Avgeris, M., Makrythanasis, P., Athanasiadis, E.I., Vamvakaris, I., Patsea, E., et al. (2021). Generation of Non-Small Cell Lung Cancer Patient-Derived Xenografts to Study Intratumor Heterogeneity. Cancers *13*, 2446.
42. Rampias, T., Karagiannis, D., Avgeris, M., Polyzos, A., Kokkalis, A., Kanaki, Z., Kousidou, E., Tzetis, M., Kanavakis, E., Stravodimos, K., et al. (2019). The lysine-specific methyltransferase KMT2C/MLL3 regulates DNA repair components in cancer. EMBO Rep. *20*, e46821.
43. Hayashi, A., Ruppo, S., Heilbrun, E.E., Mazzoni, C., Adar, S., Yassour, M., Rmaileh, A.A., and Shaul, Y.D. (2023). GENI: A web server to identify gene set enrichments in tumor samples. Comput. Struct. Biotechnol. J. *21*, 5531–5537.
44. Papadimitriou, M.A., Levis, P., Kotronopoulos, G., Stravodimos, K., Avgeris, M., and Scorilas, A. (2023). Preoperative Cell-Free DNA (cfDNA) in Muscle-Invasive Bladder Cancer Treatment Outcome. Clin. Chem. *69*, 399–410.
45. Abaan, O.D., Polley, E.C., Davis, S.R., Zhu, Y.J., Bilke, S., Walker, R.L., Pineda, M., Gindin, Y., Jiang, Y., Reinhold, W.C., et al. (2013). The exomes of the NCI-60 panel: a genomic resource for cancer biology and systems pharmacology. Cancer Res. *73*, 4372–4382.
46. Vickers, A.J., and Elkin, E.B. (2006). Decision curve analysis: a novel method for evaluating prediction models. Med. Decis. Making *26*, 565–574.
47. Vickers, A.J., Cronin, A.M., Elkin, E.B., and Gonen, M. (2008). Extensions to decision curve analysis, a novel method for evaluating diagnostic tests, prediction models and molecular markers. BMC Med. Inf. Decis. Making *8*, 53.

OMTON, Volume *32*

Supplemental information

CDKN2A copy number alteration in bladder cancer: Integrative analysis in patient-derived xenografts and cancer patients

Maria-Alexandra Papadimitriou, Katerina-Marina Pilala, Konstantina Panoutsopoulou, Panagiotis Levis, Georgios Kotronopoulos, Zoi Kanaki, Gedeon Loules, Maria Zamanakou, Dimitrios Linardoutsos, Diamantis C. Sideris, Konstantinos Stravodimos, Apostolos Klinakis, Andreas Scorilas, and Margaritis Avgeris

Figure S1

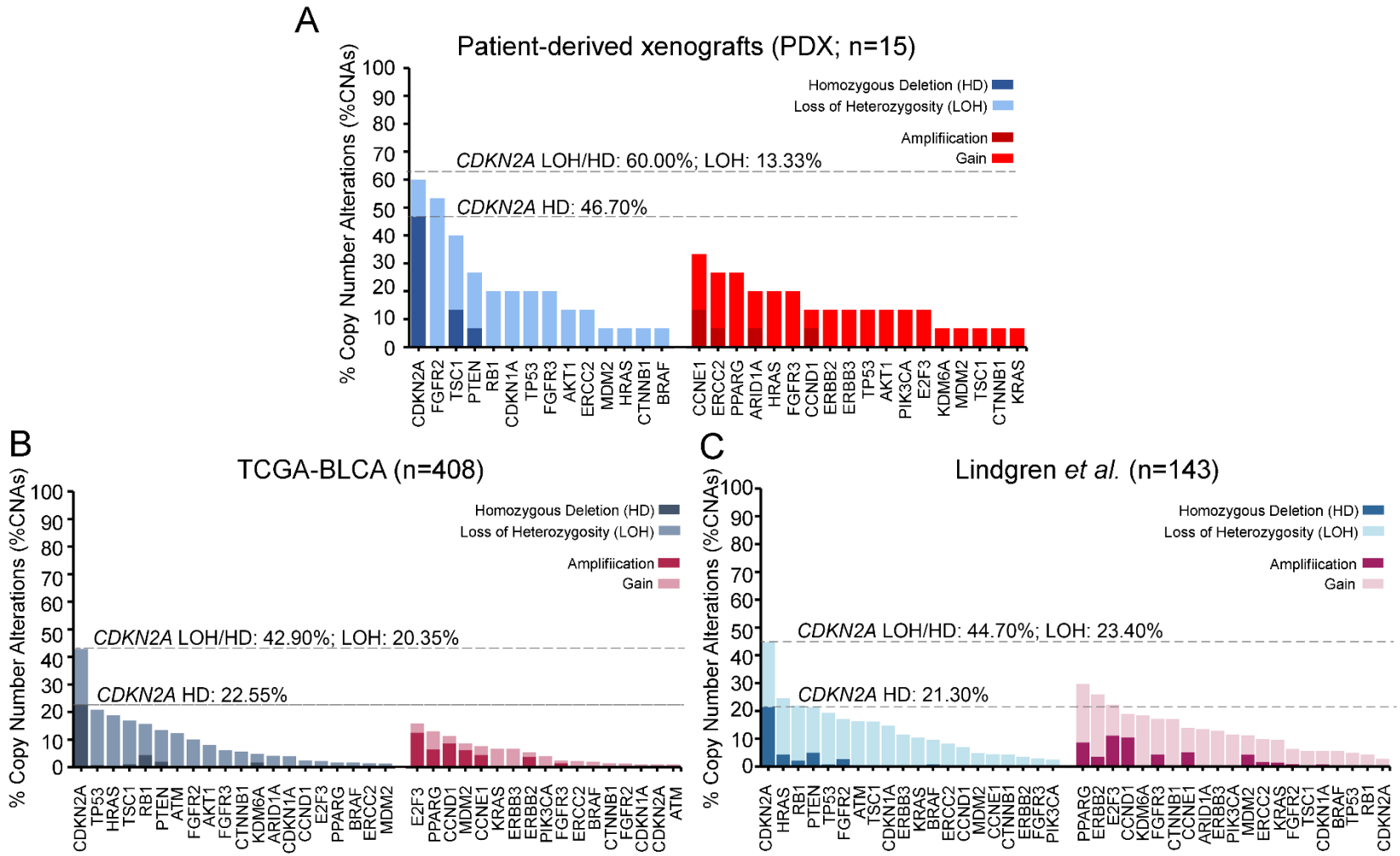

Figure S1. Bar graphs of gene level CNAs frequency (%) in PDX tumors samples (A), TCGA-BLCA dataset (B) and Lindgren *et al.* dataset (C).

Figure S2

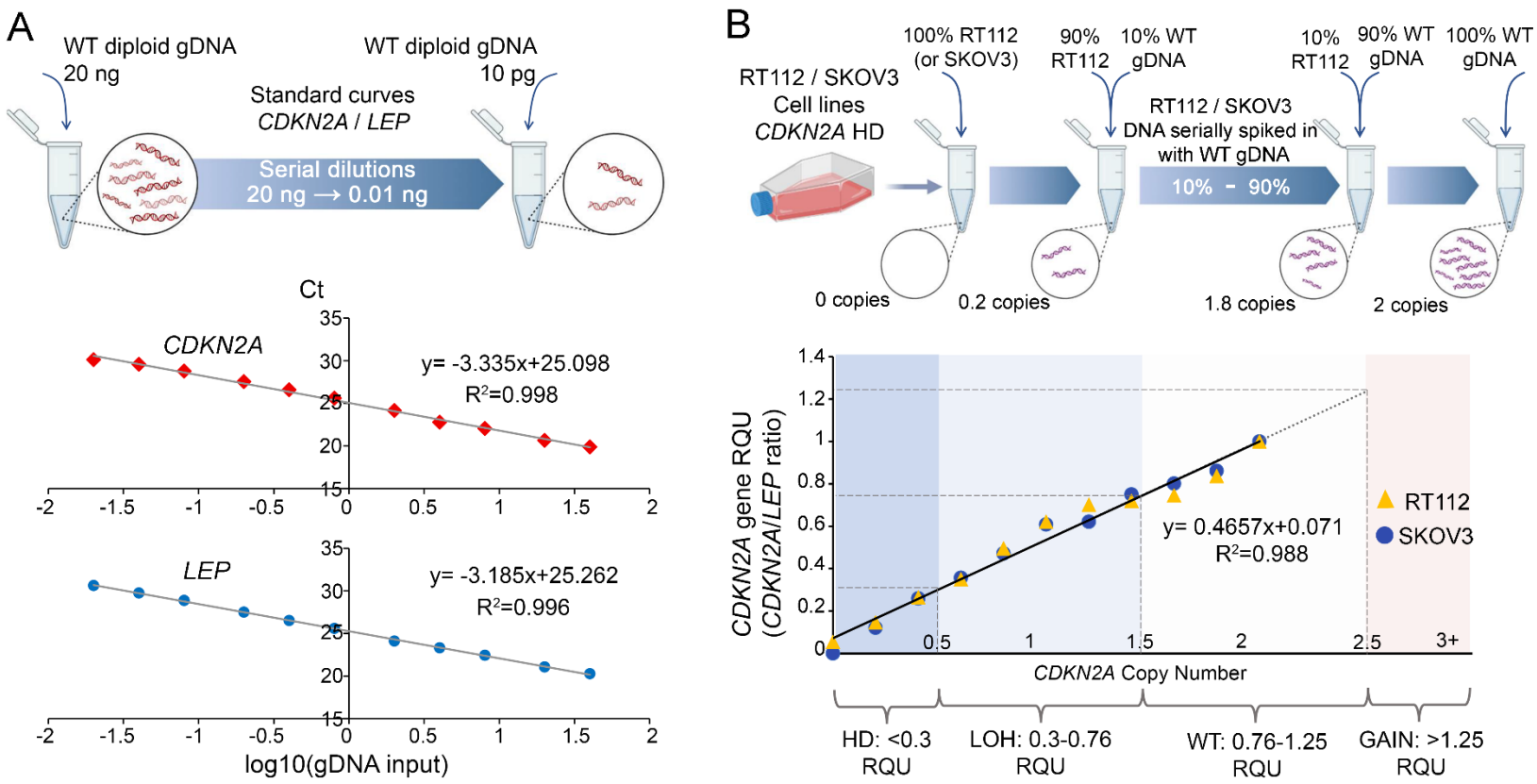

Figure S2. Development and validation of *in-house* qPCR-based method for *CDKN2A* copy-number status analysis. A. Standard curves of *CDKN2A* and *LEP* qPCR assays (range of gDNA: 0.01-20 ng). Both assays demonstrated high linearity, ensuring that PCR amplification efficiency (*CDKN2A*: E=99.9%; LEP: E=103.1%), of each target is constant over a broad concentration range. B. Standard curve for defining the optimal cut-offs for *CDKN2A* copy-number status. RT112 and SK-OV-3 cell lines, with known HD of *CDKN2A* (NCI-60/UBC-40 cell line panels) were spiked in with serially increasing amounts of *CDKN2A* diploid (wt) gDNA (0-100%). *CDKN2A* HD: *CDKN2A/LEP* ratio ≤0.30, LOH: *CDKN2A/LEP* ratio=0.30-0.76, diploid (wt): *CDKN2A/LEP* ratio =0.76-1.25, gain: *CDKN2A/LEP* ratio ≥1.25 RQU. gDNA: genomic DNA, HD: Homozygous deletion, LOH: Loss-of-heterozygosity, WT: Wild type, RQU: Relative quantitation units.

Figure S3

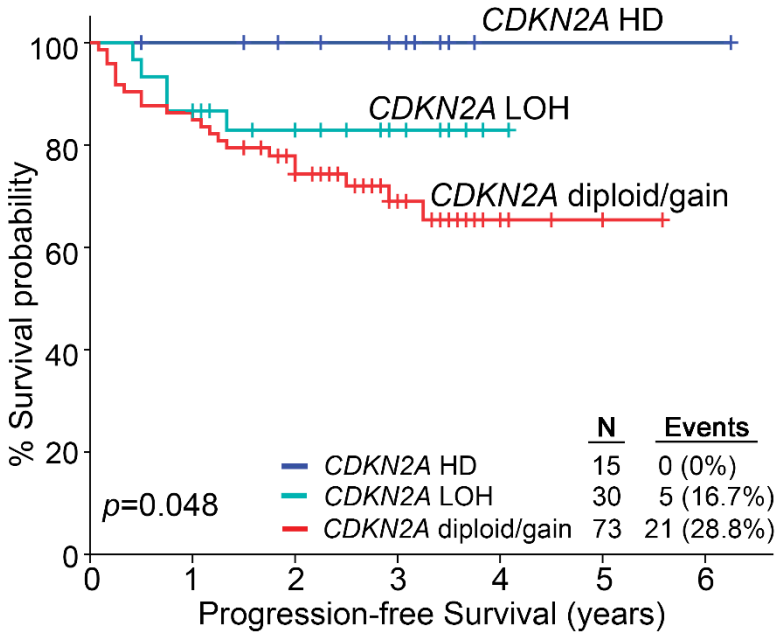

Figure S3. Kaplan-Meier survival curves for progression-free survival (PFS) of NMIBC patients according to HD *vs.* LOH *vs.* diploid/gain *CDKN2A* copy-number status. *p*-values calculated by log-rank test. HD: Homozygous deletion, LOH: Loss-of-heterozygosity

Figure S4

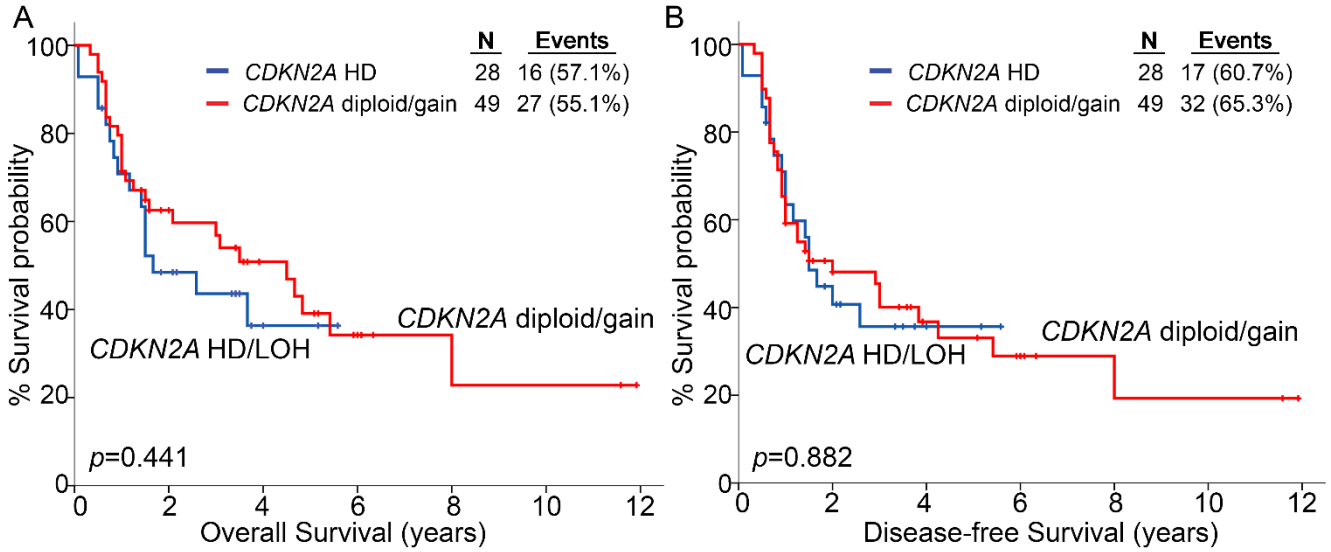

Figure S4. Kaplan-Meier survival curves for overall survival (OS) and Disease-free survival (DFS) of MIBC patients. *p*-values calculated by log-rank test. HD: Homozygous deletion; LOH: Loss-of-heterozygosity.

Figure S5

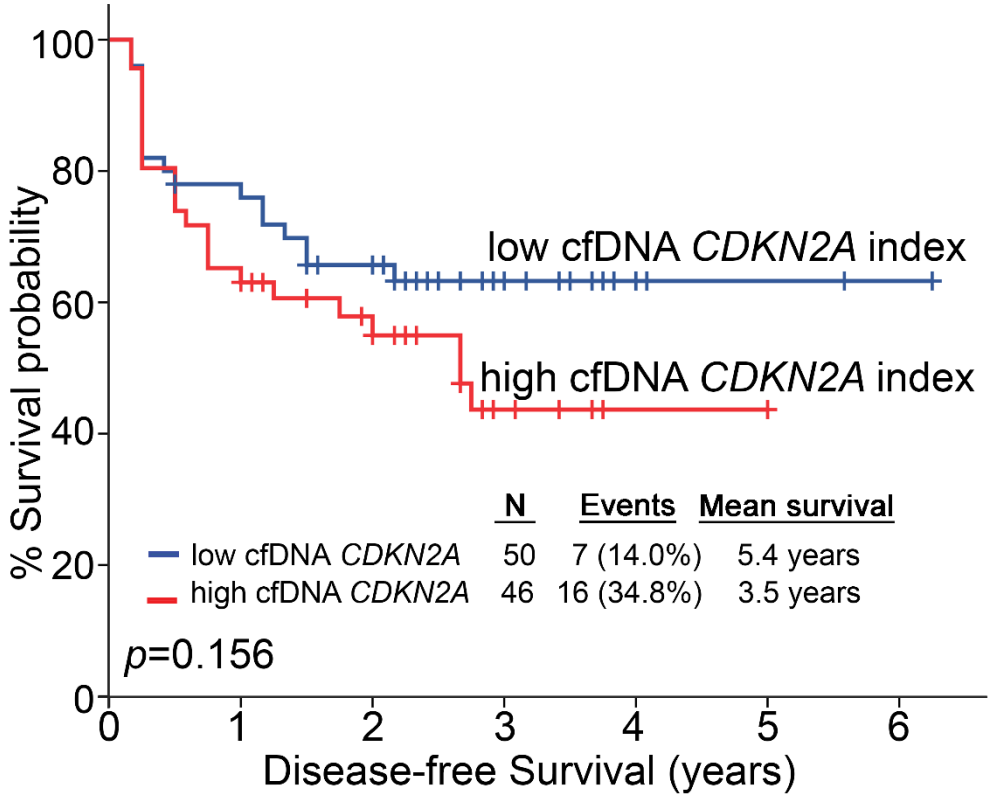

Figure S5. Kaplan-Meier survival curve for the disease-free survival (DFS) of NMIBC patients according to cfDNA *CDKN2A* index. *p*-values calculated by log-rank test. cfDNA: cell-free DNA.

Table S1. Cox regression analysis for the prediction of NMIBC (TaT1) patients' risk for relapse (DFS) and progression to invasive tumors (PFS) following TURBT according to tumor *CDKN2A* CNA status.

	Univariate analysis									
	Progression-free survival (PFS)					**Disease-free survival (DFS)**				
Covariant	**HR[a]**	**95% CI[b]**	***p*-value[c]**	**Bootstrap BCa 95% CI[d]**	**Bootstrap *p*-value[c]**	**HR[a]**	**95% CI[b]**	***p*-value[c]**	**Bootstrap BCa 95% CI[d]**	**Bootstrap *p*-value[c]**
***CDKN2A* CNA**										
Loss	1.00					1.00				
Diploid/gain	2.834	1.068 – 7.523	0.037	1.242 – 12.516	0.018	2.168	1.129 – 4.163	0.020	1.229 – 4.610	0.010
Tumor Stage										
Ta	1.00					1.00				
T1	1.685	0.773 – 3.669	0.189	0.732 – 3.971	0.168	1.371	0.783 – 2.402	0.270	0.795 – 2.373	0.267
Tumor Grade										
Low	1.00					1.00				
High	2.244	1.037 – 4.853	0.040	1.026 – 5.202	0.033	1.493	0.848 – 2.632	0.165	0.850 – 2.613	0.140
Age (continuous)	1.013	0.973 – 1.054	0.531	0.977 – 1.054	0.493	0.997	0.969 – 1.026	0.842	0.972 – 1.026	0.830
Gender										
Male	1.00					1.00				
Female	1.712	0.587 – 4.996	0.325	0.314 – 4.522	0.335	1.420	0.636 – 3.170	0.392	0.535 – 3.208	0.390
	Multivariate analysis[e]									
Covariant	**HR[a]**	**95% CI[b]**	***p*-value[c]**	**Bootstrap BCa 95% CI[d]**	**Bootstrap *p*-value[c]**	**HR[a]**	**95% CI[b]**	***p*-value[c]**	**Bootstrap BCa 95% CI[d]**	**Bootstrap *p*-value[c]**
***CDKN2A* CNA**										
Loss	1					1				
Diploid/gain	3.069	1.119 – 8.416	0.029	1.256 – 12.636	0.017	2.320	1.155 – 4.657	0.018	1.229 – 5.844	0.013
Tumor Stage										
Ta	1					1				
T1	0.678	0.199 – 2.313	0.535	0.177 – 2.155	0.512	1.038	0.438 – 2.461	0.933	0.365 – 2.838	0.945
Tumor Grade										
Low	1					1				
High	3.526	1.014 – 12.266	0.048	1.235 – 16.680	0.032	1.405	0.582 – 3.390	0.450	0.478 – 4.634	0.517
Age (continuous)	1.023	0.979 – 1.070	0.311	0.980 – 1.083	0.308	1.000	0.970 – 1.031	0.992	0.971 – 1.031	0.990
Gender										
Male	1					1				
Female	1.200	0.347 – 4.154	0.774	0.000 – 4.301	0.764	1.001	0.416 – 2.408	0.998	0.316 – 2.454	0.995

[a] Hazard Ratio, [b] 95% confidence interval of the estimated HR, [c] calculated by test for trend. Bootstrap *p*-value is based on 1000 bootstrap samples, [d] Bootstrap bias-corrected and accelerated 95% confidence interval of the estimated HR based on 1000 bootstrap samples, [e] Multivariate analysis adjusted for *CDKN2A* CNA status, tumors' stage, tumors' grade, patients' age and gender

Table S2. Cox regression analysis for the prediction of MIBC (T2-T4) patients' risk for relapse (DFS) and overall survival (OS) following RC according to tumor *CDKN2A* CNA status.

	Univariate analysis									
	Disease-free survival (DFS)					**Overall survival (OS)**				
Covariant	**HR[a]**	**95% CI[b]**	***p*-value[c]**	**Bootstrap BCa 95% CI[d]**	**Bootstrap *p*-value[c]**	**HR[a]**	**95% CI[b]**	***p*-value[c]**	**Bootstrap BCa 95% CI[d]**	**Bootstrap *p*-value[c]**
***CDKN2A* CNA**										
Loss	1.00					1.00				
Diploid/gain	0.957	0.528 – 1.734	0.885	0.536 – 1.651	0.864	0.784	0.419 – 1.469	0.448	0.421 – 1.511	0.451

[a] Hazard Ratio, [b] 95% confidence interval of the estimated HR, [c] calculated by test for trend. Bootstrap *p*-value is based on 1000 bootstrap samples,
[d] Bootstrap bias-corrected and accelerated 95% confidence interval of the estimated HR based on 1000 bootstrap samples

Table S3. Cox regression analysis for the prediction of NMIBC (TaT1) patients' risk for relapse (DFS) and progression to invasive tumors (PFS) following TURBT according to cfDNA *CDKN2A* index.

	Univariate analysis									
	Progression-free survival (PFS)					**Disease-free survival (DFS)**				
Covariant	**HR[a]**	**95% CI[b]**	***p*-value[c]**	**Bootstrap BCa 95% CI[d]**	**Bootstrap *p*-value[c]**	**HR[a]**	**95% CI[b]**	***p*-value[c]**	**Bootstrap BCa 95% CI[d]**	**Bootstrap *p*-value[c]**
cfDNA *CDKN2A* index										
Low	1.00					1.00				
High	2.954	1.210 – 7.210	0.017	1.191 – 9.730	0.013	1.523	0.821 – 2.825	0.182	0.839 – 2.865	0.159
Tumor Stage										
Ta	1.00					1.00				
T1	1.262	0.557 – 2.861	0.577	0.531 – 3.274	0.580	1.051	0.568 – 1.943	0.875	0.546 – 1.914	0.870
Tumor Grade										
Low	1.00					1.00				
High	1.908	0.841 – 4.327	0.122	0.746 – 4.824	0.117	1.095	0.584 – 2.053	0.776	0.575 – 2.070	0.750
Age (continuous)	1.017	0.976 – 1.059	0.418	0.979 – 1.061	0.347	0.996	0.967 – 1.026	0.803	0.969 – 1.025	0.772
Gender										
Male	1.00					1.00				
Female	0.998	0.295 – 3.373	0.997	0.041– 3.008	0.997	1.380	0.609 – 3.128	0.440	0.519 – 3.081	0.424
	Multivariate analysis[e]									
Covariant	**HR[a]**	**95% CI[b]**	***p*-value[c]**	**Bootstrap BCa 95% CI[d]**	**Bootstrap *p*-value[c]**	**HR[a]**	**95% CI[b]**	***p*-value[c]**	**Bootstrap BCa 95% CI[d]**	**Bootstrap *p*-value[c]**
cfDNA *CDKN2A* index										
Low	1.00					1.00				
High	2.616	1.040 – 6.582	0.041	1.069 – 9.062	0.039	1.480	0.773 – 2.834	0.237	0.776 – 2.986	0.255
Tumor Stage										
Ta	1.00					1.00				
T1	0.680	0.207 – 2.235	0.525	0.121– 2.151	0.497	1.039	0.433 – 2.494	0.932	0.302 – 3.298	0.951
Tumor Grade										
Low	1.00					1.00				
High	2.632	0.799 – 8.665	0.111	0.995 – 14.902	0.082	0.971	0.400 – 2.357	0.947	0.316 – 3.055	0.954
Age (continuous)	1.021	0.976 – 1.068	0.371	0.971 – 1.075	0.354	0.996	0.967 – 1.026	0.797	0.968 – 1.027	0.782
Gender										
Male	1.00					1.00				
Female	0.902	0.262– 3.109	0.870	0.000 – 3.379	0.830	1.240	0.541– 2.846	0.611	0.407– 3.183	0.599

[a] Hazard Ratio, [b] 95% confidence interval of the estimated HR, [c] calculated by test for trend. Bootstrap *p*-value is based on 1000 bootstrap samples, [d] Bootstrap bias-corrected and accelerated 95% confidence interval of the estimated HR based on 1000 bootstrap samples, [e] Multivariate analysis adjusted for cfDNA *CDKN2A* index, tumors' stage, tumors' grade, patients' age and gender

Table S4. Cox regression analysis for the prediction of MIBC (T2-T4) patients' risk for relapse (DFS) and overall survival (OS) following RC according to cfDNA *CDKN2A* index.

	Univariate analysis									
	Disease-free survival (DFS)					**Overall survival (OS)**				
Covariant	**HR[a]**	**95% CI[b]**	***p*-value[c]**	**Bootstrap BCa 95% CI[d]**	**Bootstrap *p*-value[c]**	**HR[a]**	**95% CI[b]**	***p*-value[c]**	**Bootstrap BCa 95% CI[d]**	**Bootstrap *p*-value[c]**
cfDNA *CDKN2A* index										
Low	1.00					1.00				
High	0.871	0.509 – 1.489	0.613	0.524 – 1.538	0.612	0.854	0.483 – 1.510	0.587	0.489 – 1.528	0.573

[a] Hazard Ratio, [b] 95% confidence interval of the estimated HR, [c] calculated by test for trend. Bootstrap *p*-value is based on 1000 bootstrap samples,
[d] Bootstrap bias-corrected and accelerated 95% confidence interval of the estimated HR based on 1000 bootstrap samples

Table S5. Quality control and coverage metrics of DNA-seq PDX samples

PDX samples	Total number of reads	Mean coverage depth (fold)	Coverage within target region (%)	MAPD[a]
1	1883203	2518.87	99.72	0.39441
2	2060433	2784.86	99.93	0.42698
3	2044401	2744.52	98.15	0.47766
4	915206	1289.31	99.71	0.49905
5	1772378	2389.49	100.00	0.41090
6	322959	468.93	98.09	0.58995
7	1524642	2056.76	93.01	0.47898
8	1752553	2361.70	100.00	0.38851
9	1911000	2568.20	100.00	0.39664
10	2525261	3332.68	100.00	0.40899
11	663778	896.01	99.93	0.43910
12	3448397	4558.24	100.00	0.41968
13	1305438	1810.33	100.00	0.47777
14	2375262	3120.10	99.20	0.44610
15	2684208	3549.67	100.00	0.41497

[a] MAPD: median absolute pairwise difference